

Compartmental modeling of the brain and the calculation of regional cerebral blood flow

by

MAHTA MIRZAI

A thesis submitted to the Faculty of Graduate Studies of the University of Manitoba in partial fulfillment of the requirements for the degree of

MASTER OF SCIENCE

© February 1993

Permission has been granted to the LIBRARY OF THE UNIVERSITY OF MANITOBA to lend or sell copies of this thesis, to the NATIONAL LIBRARY OF CANADA to microfilm this thesis and to lend or sell copies of the film, and to UNIVERSITY MICROFILMS to publish an abstract of this thesis.

The author reserves other publication rights, and neither the thesis nor extensive extracts from it may be printed or otherwise reproduced without the author's written permission.



National Library
of Canada

Acquisitions and
Bibliographic Services Branch

395 Wellington Street
Ottawa, Ontario
K1A 0N4

Bibliothèque nationale
du Canada

Direction des acquisitions et
des services bibliographiques

395, rue Wellington
Ottawa (Ontario)
K1A 0N4

Your file *Votre référence*

Our file *Notre référence*

The author has granted an irrevocable non-exclusive licence allowing the National Library of Canada to reproduce, loan, distribute or sell copies of his/her thesis by any means and in any form or format, making this thesis available to interested persons.

L'auteur a accordé une licence irrévocable et non exclusive permettant à la Bibliothèque nationale du Canada de reproduire, prêter, distribuer ou vendre des copies de sa thèse de quelque manière et sous quelque forme que ce soit pour mettre des exemplaires de cette thèse à la disposition des personnes intéressées.

The author retains ownership of the copyright in his/her thesis. Neither the thesis nor substantial extracts from it may be printed or otherwise reproduced without his/her permission.

L'auteur conserve la propriété du droit d'auteur qui protège sa thèse. Ni la thèse ni des extraits substantiels de celle-ci ne doivent être imprimés ou autrement reproduits sans son autorisation.

ISBN 0-315-81827-1

Canada

COMPARTMENTAL MODELING OF THE BRAIN
AND THE CALCULATION OF REGIONAL CEREBRAL BLOOD FLOW

BY

MAHTA MIRZAI

A Thesis submitted to the Faculty of Graduate Studies of the University of Manitoba in partial fulfillment of the requirements of the degree of

MASTER OF SCIENCE

(c) 1993

Permission has been granted to the LIBRARY OF THE UNIVERSITY OF MANITOBA to lend or sell copies of this Thesis, to the NATIONAL LIBRARY OF CANADA to microfilm this Thesis and to lend or sell copies of the film, and UNIVERSITY MICROFILM to publish an abstract of this Thesis.

The author reserves other publication rights, and neither the Thesis nor extensive extracts from it may be printed or otherwise reproduced without the author's written permission.

ABSTRACT

d,l-Hexamethyl-propylenamine-oxime (*HMPAO*) labeled with $Tc-99m$ has previously been developed as a "chemical microsphere" for imaging regional cerebral blood flow ($rCBF$) with *SPECT*. This research project consisted of computer simulation of the measurement of regional cerebral blood flow using $Tc-99m-HMPAO$. Time course data of total brain activity and arterial blood activity of the tracer were fitted to a four compartmental model: Values of the blood flow, the clearance of $Tc-99m-HMPAO$ by tissue, and the first order rate constants for back diffusion of the tracer from tissue to blood, conversion of the lipophilic tracer to the hydrophilic tracer in tissue, and conversion of the diffusible tracer to the nondiffusible one in blood were determined. Conversion of lipophilic tracer to a hydrophilic form in both blood and tissue was assumed to be irreversible.

The compartmental model together with typical rate constants, were used to generate blood and tissue tracer time activity curves. The addition of Gaussian noise to the simulated total time activity curve and the use of non-linear regression analysis allowed the determination of the mean and distribution of the computed regional cerebral blood flow. By varying the amount of added noise, the accuracy and precision of the computed regional cerebral blood flow were evaluated.

ACKNOWLEDGEMENTS

I would like to express my sincere gratitude to Dr. Roger Palser, advisor and friend, for his counsel, guideness and continuous encouragement over the course of this work.

Special thanks to my parents for their continuous support and consideration, during my study in Canada.

Extended thanks to my husband', Hamid, for his kindness and words of encouragement during my M.Sc. program, which made this work possible.

Special acknowledgments go to my colleague and friend Mrs. Y. McLellan, for many valuable comments and helpful discussions.

TABLE OF CONTENTS

Abstract	i
Acknowledgements	ii
Table of Contents	iii
List of Tables	v
List of Figures	vi
Chapter 1: Introduction	1
1.1 Xenon Enhanced Computed Tomography	4
1.2 Emission Computed Tomography	8
1.2.1 Positron Emission Tomography	9
1.2.2 Single Photon Emission Computed Tomography	15
1.2.2.1 Quantitative <i>SPECT</i> imaging	20
1.3 Choice of Tracer for Measuring <i>rCBF</i>	22
1.3.1 Development of Labeled Tracers	24
Chapter 2: Compartmental Analysis	29
2.1 Introduction	29
2.2 Compartmental Systems	29
2.2.1 Tracers	30
2.2.2 Compartments	31
2.3. Use of Computers in Compartmental Analysis	33
2.3.1 Computer Simulation Utilizing the <i>SAAM</i> Package	36
Chapter 3: Compartmental Modeling	38

3.1 Introduction	38
3.2 The Concept of Extraction Fraction, (E)	38
3.3 A Four Compartmental Model of The Brain	45
3.4 Related Works on The Measurement of CBF	50
3.5 Summary	55
Chapter 4: Methods and Results	57
4.1. Introduction	57
4.2. Experimental Procedure	57
4.2.1 Noise Free Experiments	57
4.2.2 Experiments with Added noise	58
4.3. Calculation of the Rate Constants and Flow with no error	59
4.4. Calculation of the Rate Constants and Flow with error	77
4.4.1 Computer Simulations with presence of noise	79
Chapter 5: Discussion and Conclusions	92
References	97

LIST OF TABLES

Table	page
4.1 Values of the fixed parameters in the four compartmental model.	61
4.2 Values of the dependent parameters in the four compartmental model.	61
4.3a Value of activity at its maximum and equilibrium level when $L(1, 2) = 0.650$ is varied from -75% to $+75\%$, keeping $L(2, 1)$, $L(3, 2)$, and $L(4, 1)$ at their initial values.	66
4.3b Value of activity at its maximum and equilibrium level when $L(2, 1) = 0.630$ is varied from -75% to $+75\%$, keeping $L(1, 2)$, $L(3, 2)$, and $L(4, 1)$ at their initial values.	66
4.3c Value of activity at its maximum and equilibrium level when $L(3, 2) = 0.970$ is varied from -75% to $+75\%$, keeping $L(1, 2)$, $L(2, 1)$, and $L(4, 1)$ at their initial values.	67
4.3d Value of activity at its maximum and equilibrium level when $L(4, 1) = 0.950$ is varied from -75% to $+75\%$, keeping $L(1, 2)$, $L(2, 1)$, and $L(3, 2)$ at their initial values.	67
4.4 % variation on the time activity curve for different SE.	79
4.5 % variation of mean blood flow for different standard errors.	81
5.1 Correspondence between the mean percentage error of the points of the total activity curves and the percentile errors of the blood flow calculations.	96

LIST OF FIGURES

Figure	page
1.1 A schematic representation of positron imaging by coincidence detection of the 511-Kev annihilation γ rays, showing the source distribution on two planes that could produce the detected events.	10
1.2 Three basic geometries for the detector assemblies of positron cameras.	11
1.3 Illustration of the concepts of longitudinal and transverse section tomography.	17
1.4 Image construction using linear superposition of back-projections.	18
1.5 Image construction of a point source using <i>LSFBP</i> .	19
1.6 <i>Tc-99m</i> complexes of <i>PnAO</i> and <i>HMPAO</i> .	28
2.1 Flow chart of a program to simulate kinetic behavior of tracers.	35
3.1 Diagram of a single capillary.	40
3.2 The developed four compartmental model of the brain.	47
3.3 Diagrammatic representation of the kinetic model for determining cerebral blood flow using <i>Tc-99m-HMPAO</i>	54
4.1 Plot of activity in compartment 1 over a period of 10 mins.	68
4.2 Plot of activity in compartment 2 over a period of 10 mins.	69
4.3 Plot of activity in compartment 3 over a period of 10 mins.	70
4.4 Plot of activity in compartment 4 over a period of 10 mins.	71
4.5 Plot of total activity of the four compartments vs time.	72
4.6 Relation between extraction efficiency and flow.	73
4.7 Graph of total activity vs time for different flows.	74
4.8a Plot of total time activity curve when $L(2, 1)$ is varied.	75
4.8b Graph of equil. level of activity vs rate constants.	76

4.9	Graph of $L(2,1)$ vs standard error.	84
4.10	Graph of flow vs standard error.	85
4.11	Blood flow distribution for the standard error of 0.005.	86
4.12	Blood flow distribution for the standard error of 0.01.	87
4.13	Blood flow distribution for the standard error of 0.05.	88
4.14	Blood flow distribution for the standard error of 0.1.	99
4.15	Blood flow distribution for the standard error of 0.5.	90
4.16	Error incurred in the measurement of the blood flow.	91

Chapter 1

Introduction

The aim of this thesis is to perform a computer simulation of the kinetics of uptake of radiopharmaceutical in the brain, and a feasibility study of *SPECT* as a technique for measuring regional cerebral blood flow (*rCBF*). The thesis contains five chapters.

The goal of this chapter is to review conceptually and concisely some of the basic issues involved in cerebral blood flow (*CBF*) studies, and to survey present capabilities. Emphasis is focused therefore on the underlying principles which describe various modeling techniques used in measurement of cerebral blood flow while avoiding the detail of the analysis. Listed throughout are representative references which deal with various specialty aspects related to this research work.

Cerebral blood flow is the volume of blood supplied to the brain per unit time per unit mass of tissue. It is one of the most important functional parameters that determines the state of health of the brain. A knowledge of its magnitude is important both in clinical research and in management of patients with various types of neurological disorders that include cerebrovascular disease, mental illness, epilepsy and migraine, dementia and others [Phelps, 1982; Greitz, 1983].

The measurement of regional cerebral blood flow (*rCBF*) has been pursued by methods generally based on kinetic models that require the administration of tracer substances and the measurement of their concentration in arterial blood and brain tissue. Most of the kinetic models used for this purpose have been based on the Fick principle [Jacquez, 1988], which states that the rate at which material crosses a plane by diffusion is proportional to the product of the area, A , and the concentration gra-

dient, $\frac{\partial c}{\partial x}$ at the plane.

$$\frac{dq}{dt} = -DA \frac{\partial c}{\partial x} \quad (1.1)$$

where D is the diffusion coefficient and dq is the amount of material diffusing in time dt . The negative sign is needed because there is a positive transfer of material when the gradient is negative.

This principle has been expanded by Kety [1951] to describe the exchange of inert gas, or freely diffusible substances, between capillary blood and tissue. Kety and Schmidt [1948] made the first quantitative measurement of brain blood flow, using the nitrous-oxide technique. The nitrous-oxide technique is based on the administration by inhalation of nitrous oxide at low concentration. An equilibrium distribution of the 15% nitrous oxide-air mixture between the brain tissue and arterial-venous system occurs within approximately 10 minutes from the onset of gas inhalation.

Under these conditions, the ratio of the concentrations of the tracer in tissue, C_i , to that in venous blood, C_v , is by definition the tissue blood partition coefficient, λ , for nitrous oxide. Thus at equilibrium C_i can also be defined as λC_v . This approach is based on the assumption that the arterial concentration of the tracer, C_a , is uniform throughout the arterial system so that C_a can be measured in any convenient artery. If the nitrous-oxide concentration can be determined at frequent time intervals in arterial and cerebral venous blood from the beginning of the inhalation of this gas, arterial and venous curves can be obtained. From these curves CBF can be calculated by application of the Fick principle.

Since the pioneering work of Kety and Schmidt [1948], several techniques for the measurement of cerebral blood flow have been developed. Scintillation counting of radioactive $Xe-133$ introduced by direct carotid injection or by inhalation, with washout curve analysis, made general flow analysis available to many institutions [Ingvar, 1978; Mallett, 1965; Obrist, 1967 & 1975]. However, the inherent lack of spatial resolution

and the inability to separate flow values at depth from superficial ones then led to the application of computed tomographic imaging with non-radioactive *Xe* gas [Posner, 1972; Lassen, 1978] and to other photon emitting tracers [Lassen, 1981; Kuhl, 1982; Herscovitch, 1983]. Some of the important techniques and related tracers are reviewed briefly below.

1.1. Xenon Enhanced Computed Tomography (*XeCT*)

Tomography refers to the cross-sectional imaging of an object from either transmission or reflection data collected by illuminating the object from many different directions [Kak, 1988]. The impact of this technique in diagnostic medicine has been quite extensive, since it has enabled doctors to view internal organs with precision and safety of the patient. One of the first medical applications utilized x-rays for forming images of tissues based on their x-ray attenuation coefficients [Kak, 1988]. More recently, however, clinical tomographic imaging has also been successfully accomplished with radioisotopes, ultrasound, and magnetic resonance; the imaging parameter being different in each case.

The purpose of *CT* is the reconstruction or synthesis of an image that faithfully represents the internal anatomy of a transverse cross-section (or slice) of the body. A large quantity of data is collected which represents the attenuation of a finely collimated x-ray beam passing at multiple angles through points within the particular cross section being imaged. This assembly of data is processed by a computer. Incorporated within the computer program is an algorithm, or procedure for reconstructing an image of the slice usually by the filtered back-projection technique. The final product is an array of CT numbers, each of which represents the linear x-ray attenuation coefficient in a small volume element within the appropriate tissue slice. Appropriate display devices can then portray each of these small volume elements in some shade of color related to its CT number.

The *XeCT* blood flow technique consists of administering stable *Xe* by inhalation and monitoring its diffusion into tissue by using time sequential computerized tomography. Because of *Xe*'s high atomic number relative to that of tissue, changes in *Xe* concentration will lead to observable changes in the *CT* number of that tissue volume. The relationship between enhancement in the *CT* number and *Xe* concentration has been described by [Lee, 1990];

$$\Delta CT(t) = \alpha C(t) \quad (1.2)$$

where $\Delta CT(t)$ is the change in CT number at time t , $C(t)$ is the concentration of Xe in the brain tissue, and α is the calibration factor of the scanner. Application of the Kety-Schmidt equation for blood flow studies requires measurement of both the concentration of Xe in cerebral arterial blood and its concentration in cerebral tissue as functions of time. For a given region i :

$$C_i(t) = f_i \int_0^t C_a(w) e^{-K_i(t-w)} dw \quad (1.3)$$

where C_i and C_a are the tissue and arterial blood Xe concentrations respectively. If K_i is the rate constant and f_i is the flow in the region then,

$$f_i = \lambda K_i \quad (1.4)$$

where λ is the tissue blood partition coefficient. As Xe is inhaled, its arterial concentration is assumed to be in equilibrium with its end-tidal concentration of Xe in expired gas [Obrist 1975]. A calibration graph, relating the Xe concentration to the change in CT number, is obtained from a separate experiment. The concentration of Xe in expired gas, from which the required estimate of $C_a(t)$ can be derived, can be monitored in different ways such as the thermoconductivity measurement method [Meyer, 1980], the subtraction method [Good, 1987], and using mass spectrometry [Herron, 1984]. Once the Xe concentration has been determined, a two parameter least squares fit to the Kety-Schmidt equation is employed at each voxel to find the rate constant K and partition coefficient λ [Good, 1987]. Evaluation of the Kety-

Schmidt equation involves numerical integration, making the optimization calculations very time consuming. One possible way of simplifying the calculation is to fit the arterial data with a function which allows the integral to be solved analytically. Good and Gur [1987] evaluated possible types and magnitude of errors in blood flow estimates introduced by the above numerical procedure. In their study comparing the use of actual arterial data to the use of a fit to the actual data, they concluded that typically the fitting procedure introduces errors in flow estimates on the order of +3% to -7%. Of all combinations of flow and partition coefficient values they considered, the most extreme flow errors occurred in cases of high flow combined with low partition coefficient (gray matter), while the least extreme errors occurred in cases of low flow and high partition coefficient (white matter). From their simulation data it was suggested that the presence of a linear component in the real arterial data will cause calculations based on a fit of the data to underestimate flow values. Underestimation of the rate constant did not cause a large overestimation of flow values. The study suggested that timing correlation between the arterial data (i.e. arrival of X_e at the brain) and the CT data was crucial. Timing errors on the order of 0.1 min can produce errors in flow estimates of as much as 14% [Good, 1987]. This timing error could result from either lack of synchronization between the two data collection systems, the response time of the X_e gas monitor, the finite time interval required for the collection of a single CT scan, or from the delay between the end-tidal X_e concentration and the actual concentration of X_e in cerebral arterial blood. The implication of timing error to this research work will be discussed in chapter four.

The improved spatial resolution provided by advanced CT permits better visualization of detail, and fast scanners enable the rapid serial imaging necessary to monitor the changes in X_e concentration over time. This will allow quantitative, *in-vivo* determination of blood flow rates in discrete anatomic locations based on the principles of inert gas exchange between blood and tissues set by Kety [1951]. Although CT

provides good spatial resolution, certain limitations exist when performing quantitative studies. The technique is an invasive procedure, and since Xe is an anesthetic gas, more intensive medical support is needed than in some other techniques. Problems associated with $XeCT$ studies are radiation dose, patient motion, as well as Xe side effects [Wolfson, 1982]. Another limiting factor in obtaining better image quality is the statistical noise [Good, 1987]. This problem can be partially solved by increasing scan times (more radiation) and picture element (pixel) size, but both of these alternatives are objectionable. Increasing scan times increases patient radiation exposure and increasing the pixel or voxel size decreases the spatial resolution [Bews, 1990].

1.2. Emission Computed Tomography

In conventional x -ray tomography, physicians usually use the attenuation coefficient of tissue to infer diagnostic information about the patient. Emission CT , on the other hand, uses the decay of radioactive isotopes to image the distribution of the isotope. These isotopes may be administered to the patient in the form of radiopharmaceuticals either by injection or by inhalation. Thus, for example, by administering a radioactive isotope by inhalation, emission CT can in principle be used to trace the path of the isotope through the lungs and the rest of the body.

Radioactive isotopes useful in blood flow studies are characterized by the emission of gamma-ray photons or positrons, both products of nuclear decay. The concentration of such an isotope in any cross-section changes with time due to radioactive decay, flow, and biochemical kinetics within the body. This implies that all the data for one cross-sectional image must be collected in a time interval that is short compared to the time constant associated with the changing concentration. But then this aspect also gives emission CT its greatest potential and utility in diagnostic medicine, because now by analyzing the images taken at different times for the same cross section one can determine the functional state of various organs in a patient's body. Emission CT is of two types : single photon emission CT ($SPECT$) and positron emission CT (PET). The word single in the former refers to the product of the radioactive decay, a single photon, while in positron emission CT the decay produces a single positron which decays to two photons. In the following sections these methods and the related techniques are briefly discussed.

1.2.1. Positron Emission Tomography (*PET*)

With positron emission tomography (*PET*), one wants to determine the concentration and location of a positron emitting compound in a desired cross section of the human body. *PET* is based on the principle of annihilation coincidence detection. When a positron is emitted from a radionuclide within the body, it will travel only a short distance (of the order of 1 mm) before annihilating with an electron to produce two 511 keV photons that are emitted in opposite directions.

In *PET* there are two detectors opposite to one another. A coincidence detector records an event only in response to gamma rays being received at both detectors (Fig. 1.1). This establishes an "electronic" collimation and eliminates the need for the conventional absorption collimators. Deletion of the collimator significantly increases the number of photons available for image formation. The two detectors measure coincidences from all the activity in a line joining them, i.e., for a general activity distribution they measure a line integral through the distribution. If all possible line integrals through a given plane are measured, then the distribution of activity in the plane may be reconstructed using a filtered back-projection technique [Harbert, 1984]. Ideally, an imaging device utilizing the annihilation coincidence detection technique should measure all possible line integrals through a plane of the body. There are many possible detector configurations that achieve this goal. Three approaches to detector geometry have been followed in commercially available *PET* systems. These approaches are classified as parallel-opposed multicrystal array, hexagonal arrays and circular tomographic units which are shown in Fig 1.2 [Hendee, 1983]. By far the most popular design is to have a stationary circular ring of discrete detectors, usually small Bismuth Germanate detectors (*BGO*), each one operating in coincidence with many opposing detectors as shown in Fig. 1.2c. *BGO* detectors are used because the greater physical density of *BGO* compared to sodium iodide (*NaI*) yields increased absorption of incident annihilation photons.

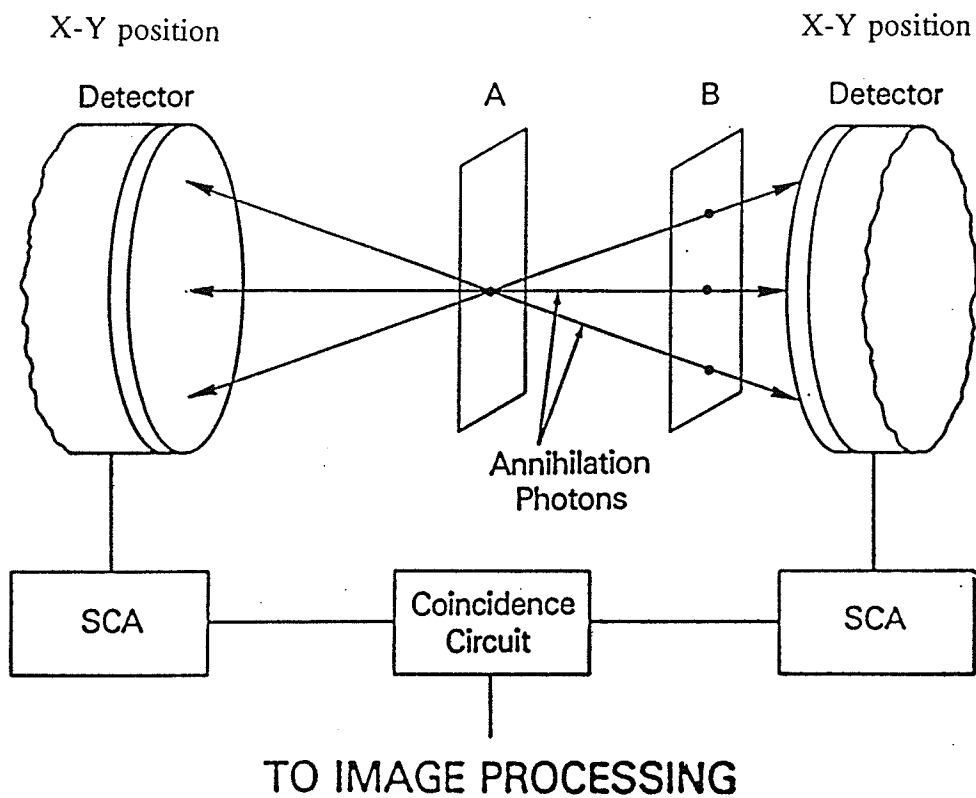


Fig. 1.1 : A schematic representation of positron imaging by coincidence detection of the 511-Kev annihilation γ rays, showing the source distribution on two planes that could produce the detected events [Harbert, 1984].

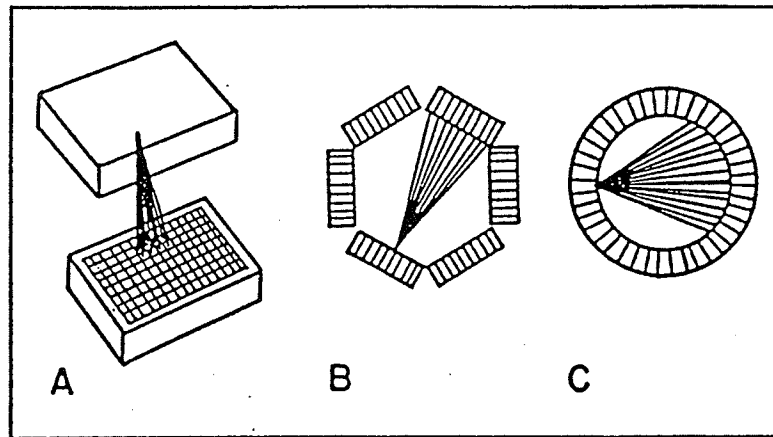


Fig. 1.2 : Three basic geometries for the detector assemblies of positron cameras.

A. Parallel opposed detectors. B. Hexagonal arrays. C. Circular tomographic units composed of a single ring or multiple rings of detectors [Hendee, 1983].

Different techniques have been developed to provide multisection capability. The most popular design is the use of more than one ring of detectors surrounding the patient which offers several advantages over the alternative designs [Hendee, 1983]. Among these advantages are increased sensitivity and the capability of producing many tomographic sections simultaneously. The spatial resolution of ring-detector cameras currently is of the order of 7 to 8 mm.

PET has been applied in the studies of normal cerebral function and in clinical studies of several pathologic conditions [Phelps, 1982]. By using tracer kinetic models parameters such as *CBF* can be measured. Several tracers have been proposed for the measurement of *rCBF* with *PET*. In clinical applications, however, the most common tracers used for flow measurements have been $H_2^{15}O$ and $C^{15}O_2$ [Raichle, 1983]. $H_2^{15}O$ has been administered intravenously and $C^{15}O_2$ is administered by inhalation. In the latter case the *O*-15 label is rapidly transferred to the water pool in the lung capillary bed [West, 1962]. $H_2^{15}O$ has several desirable characteristics for blood flow measurement. For instance, water is a biologically inert, naturally occurring compound and $H_2^{15}O$ has no undesirable physiologic side effects. Because of the short half life of *O*-15, relatively large amounts of radioactivity can be administered to obtain good images.

A possible drawback of $H_2^{15}O$ is the fact that water is not strictly freely diffusible [Eichling, 1974]. This might lead to underestimation of *rCBF* at high flow rates. However, in humans the underestimation of *rCBF* for normal or decreased flow is expected to be small [Lammertsma, 1981].

Methods for measuring *rCBF* with *PET* are based on the approach developed by Kety [1948] to describe the *in-vivo* behavior of inert, diffusible flow tracers. There are several different techniques for measuring *rCBF* with *PET* and all are based on the Fick principle:

$$\frac{dC_i}{dt} = f \left(C_a - \frac{C_i}{\lambda} \right) \quad (1.5)$$

where C_i and C_a are the concentrations of tracer in tissue and in arterial blood, respectively.

Four main methods have been used to measure $rCBF$ with $H_2^{15}O$ and $C^{15}O_2$ utilizing *PET*. The steady-state technique [Subramanyam, 1978], the integrated projection technique [Huang, 1983], the autoradiographic technique [Raichle, 1983, Kanno, 1984], and the dynamic technique [Lammertsma, 1981]. The steady-state and dynamic techniques both utilize continuous inhalation of $C^{15}O_2$, and the other two methods use a bolus intravenous injection of $H_2^{15}O$ [Kannao, 1984]. Each of these methods has its relative advantages and limitations. For example, the steady-state technique has low temporal resolution, is statistically vulnerable to changes at high flow values [Lammertsma, 1981], and makes inefficient use of the total radioactivity administered to the subject. The autoradiographic and integrated projection techniques produce results that are reported to be scan time dependent [Raichle, 1983]. This is probably because they do not take into account delay and dispersion of the measured arterial blood curve relative to the recorded tissue data [Lammertsma, 1981]. The scan time dependency of the autoradiographic technique may also result from using an incorrect value for the volume of distribution of water, upon which the later phase of the data is dependent.

Recently a dynamic method, the build-up technique [Lammertsma, 1989], has been described, which performs an intrinsic correction for the delay and dispersion of the measured arterial blood curve. This build-up technique provides CBF values that are independent of study duration [Lammertsma, 1989]. The disadvantages of this method are a relatively long scan duration (10min) and the fact that, owing to noise considerations, results are obtained for an arterial whole-blood time activity curve, without producing a quantitative CBF image. However, Lammertsma [1990] has

modified the buildup technique to provide additional features. In his work, the study duration is reduced to 3 min and a functional *CBF* image is obtained using an additional integral analysis. The accuracy of the method is based on the $C^{15}O_2$ buildup technique as it was described in his earlier work [Lammertsma, 1989].

In summary, *PET* is one of the most accurate techniques designed to give regional quantitative information on brain perfusion. Compared to other modalities, *PET* remains very expensive, generally unavailable on a routine basis for clinical investigation of patients, and is at present installed in a very limited number of centers.

1.2.2. Single Photon Emission Computed Tomography (*SPECT*)

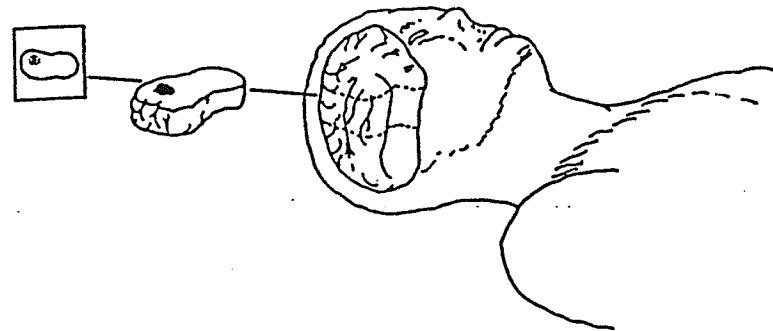
In conventional radionuclide imaging techniques the collected data is two dimensional with no information obtained about the depth of the source within the patient. To provide information about the third dimension, depth, Single Photon Emission Computed Tomography techniques were introduced (*SPECT*). There are two approaches to *SPECT*, namely longitudinal and transverse [Hendee, 1983, Ell, 1987].

In the first approach, longitudinal tomography, images are formed in planes parallel to the surface of the detector and to the axis of the body as shown in Fig. 1.3a. taken from Nudelman, 1980. To generate such images the trajectory of the detector relative to the patient is similar to that used in conventional radiographic tomography. The longitudinal section images are thus inherently low in contrast due to the fact that activity in planes outside of the plane of interest interfere with data collection from the plane of interest.

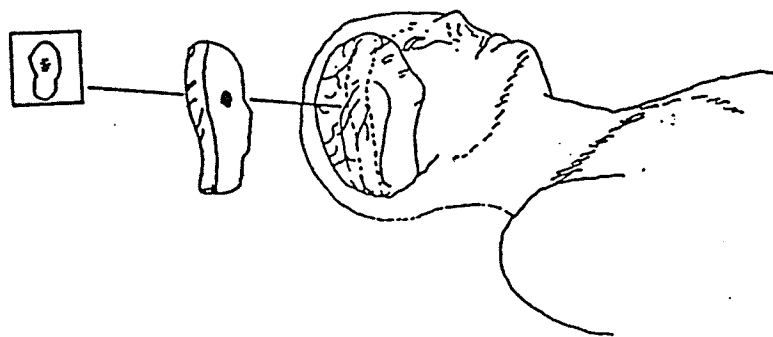
The second approach (transverse tomography) provides images perpendicular to the detector surfaces by a technique analogous to that of *x-ray CT*. Thus the transverse images do not suffer from noise interference by adjacent slices. Transverse imaging is accomplished by recording data from the patient from many different angles by rotating the detector about the patient. Image reconstruction is then accomplished by projecting the data back along lines through the image corresponding to the direction from which the data were collected, as in Fig. 1.4. Fig. 1.4, illustrates the case of a point source. When the point source is scanned at various angles, (1.4a) a set of projections (1.4b) are obtained. Each projection indicates the position of the point source in the plane of the projection. However, the source could be anywhere along the line passing through the point source and perpendicular to the projection. The information from each projection is then back projected along the line across the whole image (Fig. 1.4c). When the back projections of all the scans are then added together, an approximation of the original object distribution results [Mcfarlane, 1988]. This method of

obtaining an image is known as linear superposition of back projections (*LSBP*) [Sorenson, 1980]. As shown in Fig. 1.4c the image is considerably blurred. Blurring, however, can be decreased but not eliminated by increasing the total number of projections. To eliminate the blurring a linear superposition of filtered back-projections (*LSFBP*) can be used [Sorenson, 1980]. In *LSFBP* the projections are first modified by a filtering technique (Fig. 1.5) to yield an exact reconstruction method which produces sharp, quantitative images, whereas the *LSBP* technique produces blurred inaccurate images.

The sensitivity may be improved by the addition of more camera heads. A dual-headed system with two detectors mounted opposite each other can half the examination time. Also, there are triple-headed systems with improved geometry, electronics and collimators that can reduce imaging times by about a factor of five.

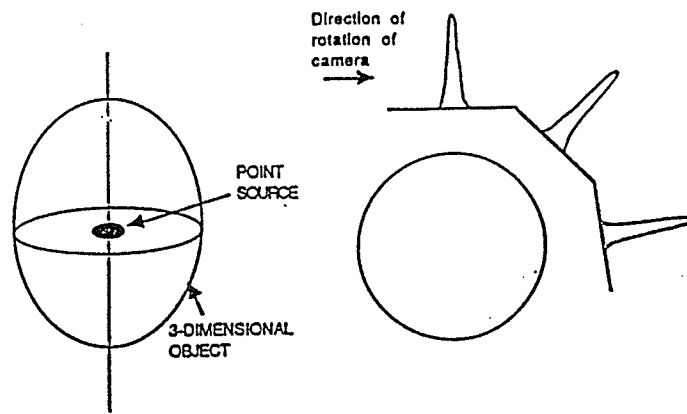


A. LONGITUDINAL SECTION



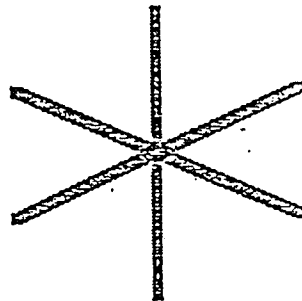
B. TRANSVERSE SECTION

Fig 1.3 : Illustration of the concepts of longitudinal and transverse section tomography
[Nudelman, 1980].



(a) POINT SOURCE EMBEDDED IN A 3-DIMENSIONAL OBJECT

(b) TO ILLUSTRATE HOW THE CAMERA SCANS OBJECT, OBTAINING PROFILES AT VARIOUS ANGLES



(c) BACKPROJECTION, AND SUPERPOSITION OF PROFILES TO OBTAIN AN APPROXIMATION TO THE ORIGINAL SOURCE DISTRIBUTION

Fig 1.4 : Image construction using linear superposition of back-projections

[McFarlane, 1988].

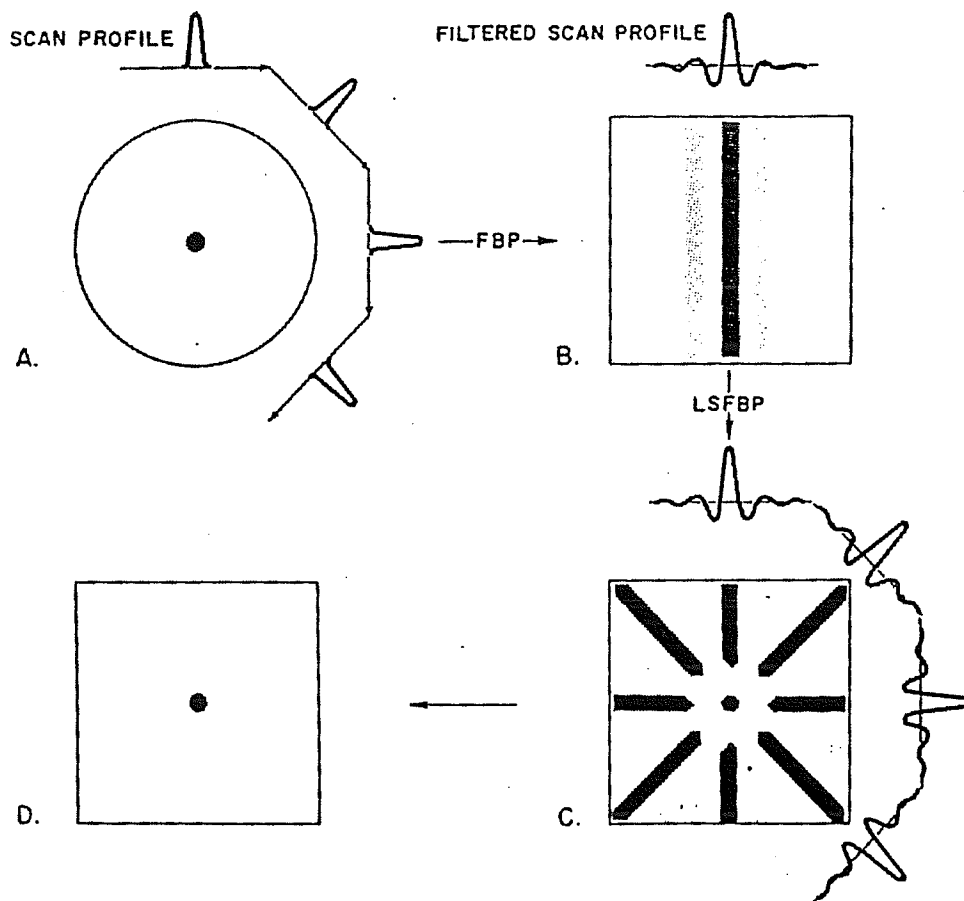


Fig 1.5 : Principle of linear superposition of filtered backprojection (*LSFBP*). (A) Object and scan profiles. (B) Single filtered scan profile projected back cross image. (C) Four filtered scan profiles projected back across image and added together (superposition). (D) Image produced when sufficient angles are employed to remove residual components outside the image of the central object [Sorenson, 1980].

1.2.2.1. Quantitative SPECT Imaging

The aim of quantitative *SPECT* imaging is to determine the radiopharmaceutical concentration inside a body organ by measuring the photon flux outside the body. However, there are certain physical problems associated with *SPECT* which limit the accuracy of quantitation.

Between the point of emission and detection, photons may undergo scattering and attenuating processes. The name Compton scattering is given to a collision between a photon, and a loosely bound outer shell orbital electron. As a result of the collision, the photon loses part of its energy to the electron, which then recoils, and the photon is deflected from its original path. If the energy of this scattered photon is still within the photopeak window, it will be included in the final *SPECT* image. Therefore, an effect of scatter is to include some scattered photons in the final image, and to alter the distribution of energies of radiation striking the detector. As a result, lesion contrast and spatial resolution are decreased, making it more difficult not only to detect the lesions, but also to locate the lesion border. On the other hand, attenuating processes cause photons to be removed from the final image. The amount of attenuation depends on the photon energy and the thickness and the composition of the matter through which it passes. Correction for the effects of scatter and attenuation have been identified as the most difficult problem associated with accurate *SPECT* quantitation [Parker, 1989].

An iterative post-processing technique for correction of both scatter and attenuation in *SPECT* was reported by Axelsson [1984]. A primary uncorrected image was used to estimate the effect of attenuation on measured projected data. The method used in Axelsson's work is based on the assumption that the measured projection data are a sum of primary and scattered photons and that the scattered component could be estimated by convolving the measured projection data with a scatter distribution function obtained from measuring the line-spread function of the detector. The scatter-

corrected projection data were then used as input data for the attenuation correction. The corrected projection data were used in the final reconstruction. The post-processing technique could be repeated in several iterations. The convergence rate was very fast and less than two iterations were needed to obtain results with a high degree of accuracy. The purpose was to allow the user to select the less accurate but fast pre-reconstruction method for routine qualitative imaging, and use the more time-consuming post-reconstruction algorithm only if needed. The results of Nickel, 1989, show that this algebraic attenuation correction technique can determine *in-vivo* count distributions with an accuracy of $\pm 10\%$.

An alternative but less accurate method to relate the radiopharmaceutical concentration in an organ to the regional count density is an image, is to perform a phantom study and generate a calibration graph. The procedure for this calibration is that a known amount of activity is injected into a phantom and scanned. The process of image reconstruction is carried out the same way as it is done in the case of a patient study. Regions of interest (*ROI*) in the phantom image are set up to obtain total counts for each region. This procedure can be repeated for different amounts of activity given to the phantom. A graph of total counts versus the radiopharmaceutical concentration can be obtained and plotted. This graph is then used as a calibration for the clinical image. Clearly the accuracy of the calibration will depend upon how closely the phantom mimics the patient. Thus, regional activity distributions can be determined to an accuracy of about 10%, and as will be discussed later, used in flow and rate constant calculations.

1.3. Choice of Tracer for Measuring $rCBF$ with *SPECT*

The study of $rCBF$ by means of *SPECT* has received widespread attention in the past decade. The ideal radiopharmaceutical for assessing $rCBF$ should distribute proportional to flow, freely cross the intact blood brain barrier (*BBB*), i.e., the barrier separating the blood from the brain parenchyma every where except in the hypothalamus, and distribute proportional to blood flow, and retain its fixed regional distribution in the brain for a period of time sufficient to permit image acquisition (20-30 min for a rotating, single headed gamma camera [English, 1986]. It should also be chemically and radiologically safe, and permit repeated studies, be widely available and preferably inexpensive.

The important technique for *SPECT* studies of $rCBF$ is the *chemical microsphere* technique [Lucignani, 1985]. Several radioactive tracers have been proposed for this purpose and their concentrations are monitored either by external detectors for use in human beings or quantitative autoradiography for studies in animals [Sakurada, 1978]. It should be noted that the above mentioned "chemical microspheres" are different from the radioactive microspheres [Biersack, 1990]. The latter, are tracers which are physical particles and remain physically trapped in the capillary bed because of their size. They are generally used for experiments in animals by direct intracardiac injection, not intravenous injection. The measurement of tissue concentration of these tracers can be performed over an interval of time since their level remains essentially constant.

The intravenous route, on the other hand, is feasible with "chemical microspheres". These are soluble molecules which can diffuse freely across the capillary bed and are trapped in tissue on the basis of some chemical mechanism. For these tracers, the tissue concentration changes throughout the experimental time and its measurement has to be performed over a short interval. The selection of the proper tracer and system used for recording the activity are of critical importance to obtaining

meaningful information on brain physiology. Therefore, in the next section a discussion on the available tracers is presented.

1.3.1. Development of Labeled Tracers

Over the last decade, several brain imaging radiopharmaceuticals have been developed that permit routine *rCBF* imaging by *SPECT*.

Winchell and Baldwin [1980] and Tramposch [1983] have investigated many iodophenylalkyl amines labeled with radioactive iodine in search of a flow tracer that could cross the intact *BBB* and remain trapped inside the brain tissue, i.e., *chemical microsphere*. Two iodinated chemical microspheres which have been most widely tested and used for *rCBF* assessment are isopropylidoamphetamine (*IMP*) and N, N', N'-trimethyl-N-(2-hydroxy-3-methyliodobenzyl)-1,3- propane- diamine (*HIPDM*). The biodistribution and the kinetics of these tracers have been studied in animals and man in order to design quantitative methods for *rCBF* measurements [Holman, 1984; Lear, 1982].

As with other compounds which do not have active transport systems, the penetration of the *BBB* by these tracers is attributed to free diffusion of the un-ionized lipophilic form of the compound. In particular, the mechanism of uptake and retention of *IMP* has been attributed to its lipophilicity and affinity for high-capacity, relatively nonspecific binding sites in brain and capillary endothelium. For *HIPDM* the mechanism of trapping has been attributed instead to a change from the un-ionized to ionized form in the passage across the *BBB* due to the difference in *pH* between blood and brain tissue [Kung, 1980].

Both *IMP* and *HIPDM* have been reported to be distributed in brain in proportion to blood flow. Although this represents a necessary condition for measurement of *rCBF* with any tracer, it is not enough. Additionally, the tracer must distribute proportional to blood flow and must cross the *BBB* and be completely extracted from the blood into brain tissue during a single passage through the brain capillaries. Under these conditions *rCBF* can be measured. The results of studies done on animals and humans indicate that *HIPDM* is not suitable for quantitative measurement of *rCBF*

with the indicator distribution method. Observations suggested that a steady-state bi-directional flux of *HIPDM* between blood and brain tissue was occurring rather than a complete irreversible trapping of this compound in the brain. However the tissue equilibrium model, which assumes bidirectional exchange between the tissue and the blood, can be used. The tissue equilibration method, although more suitable, still represents a relatively unsatisfactory alternative because of the need to know the kinetic constants and metabolic degradation of *HIPDM* in each study in humans. Both the kinetic constants and the rate of *HIPDM* metabolic degradation could vary among individuals and in pathological conditions [Winchell, Baldwin, 1980].

A more acceptable and economic approach would be to use *Tc-99m* labeled agents that would cross the intact *BBB*. Since *Tc-99m* has a shorter half life (6.6h compared to 13.3h) better imaging characteristics than *I-123* and lower radioactivity [Leonard, 1986] one can use more activity of *Tc-99m* and thus obtain better images than with *I-123*. Also *Tc-99m* is less expensive and more readily available. However, the basic problem with *Tc-99m* is how to incorporate the radionuclide into an organic molecule so that a lipophilic complex is formed that rapidly crosses the blood brain barrier (*BBB*) and is retained in the brain. Most work has centered on derivatives of propylene amine oxime (*PnAO*) proposed by Troutner [1983] and on the diamino-dithiols (*BAT*) proposed independently by Kung [1983] as well as Ravert [1983]. These initial efforts were successful in that rapid uptake into the brain was demonstrated with some but not all of these lipophilic compounds. A major problem with this first set of *Tc-99m* brain imaging compounds was that some of them demonstrated either a high degree of plasma protein binding and did not appreciably cross the *BBB* or, if they did cross the *BBB*, they were not retained due to rapid back-diffusion (brain to blood). Thus *SPECT* images, requiring stability for periods of 20 to 30 minutes, could not be obtained with a rotating gamma camera.

The evaluation of a large number of *PnAO* derivatives led to the selection of *Tc-99m-HMPAO* [Neirinckx, 1986] (figure 1.6) as a promising complex. Like *Tc-99m-PnAO*, *Tc-99m-HMPAO* is neutral and lipophilic, but is not stable in aqueous solution. Freshly prepared solutions of *Tc-99m-HMPAO* contain greater than 90% of the desired, neutral lipophilic complex.

The *Tc-99m-HMPAO* ligand exists in two diastereoisomeric forms, *d,l* and *meso*. Both complexes are neutral, lipophilic, and unstable. The *d,l* complex is more unstable than the *meso* complex. When the *d,l* complex is administered intravenously, approximately 70–80% of the primary complex reaching the brain crosses the *BBB* [Andersen, 1988]. Once the primary complex has crossed the *BBB*, its fate is determined by the competition between a rapid conversion to a non-diffusible form and washout to blood.

While the original clinical studies with *Tc-99m-HMPAO* were conducted with a mixture of these two forms it was shown in rats [Nowotnik, 1985] and humans [Sharp, 1986] that *d,l-HMPAO*, provides a *Tc-99m* complex with superior brain uptake and retention compared with the mixture. The clinical use of this agent has spread very rapidly and it has been introduced as an alternative to the other agents, i.e. *I-123* labeled complexes, for measurement of *rCBF*. Therefore, in this research work *Tc-99m-HMPAO* was selected as the tracer for the study of *rCBF*.

It should be also noted that Cheesman [1988] has developed a number of *Tc-99m* complexes of ester derivatized *DADT* ligands. Of these compounds *Tc-99m-N, N'-1,2-ethylenediylbis-L-cysteine* diethyl ester (*ECD*) has shown excellent uptake and retention characteristics for *SPECT* imaging in primates [Walovitch, 1988]. Vallabhajosula [1989] has studied the *in-vivo* kinetics and biodistribution of *ECD* in normal subjects. He found that *Tc-99m-ECD* is rapidly taken up by the human brain. The biodistribution studies reported by Vallabhajosula [1989] were to evaluate the safety of *ECD*. The protocol did not include brain *SPECT* imaging stu-

dies. It was therefore difficult to infer from the biodistribution studies if $Tc-99m-ECD$ brain uptake reflects $rCBF$. Therefore it was not selected for this research study.

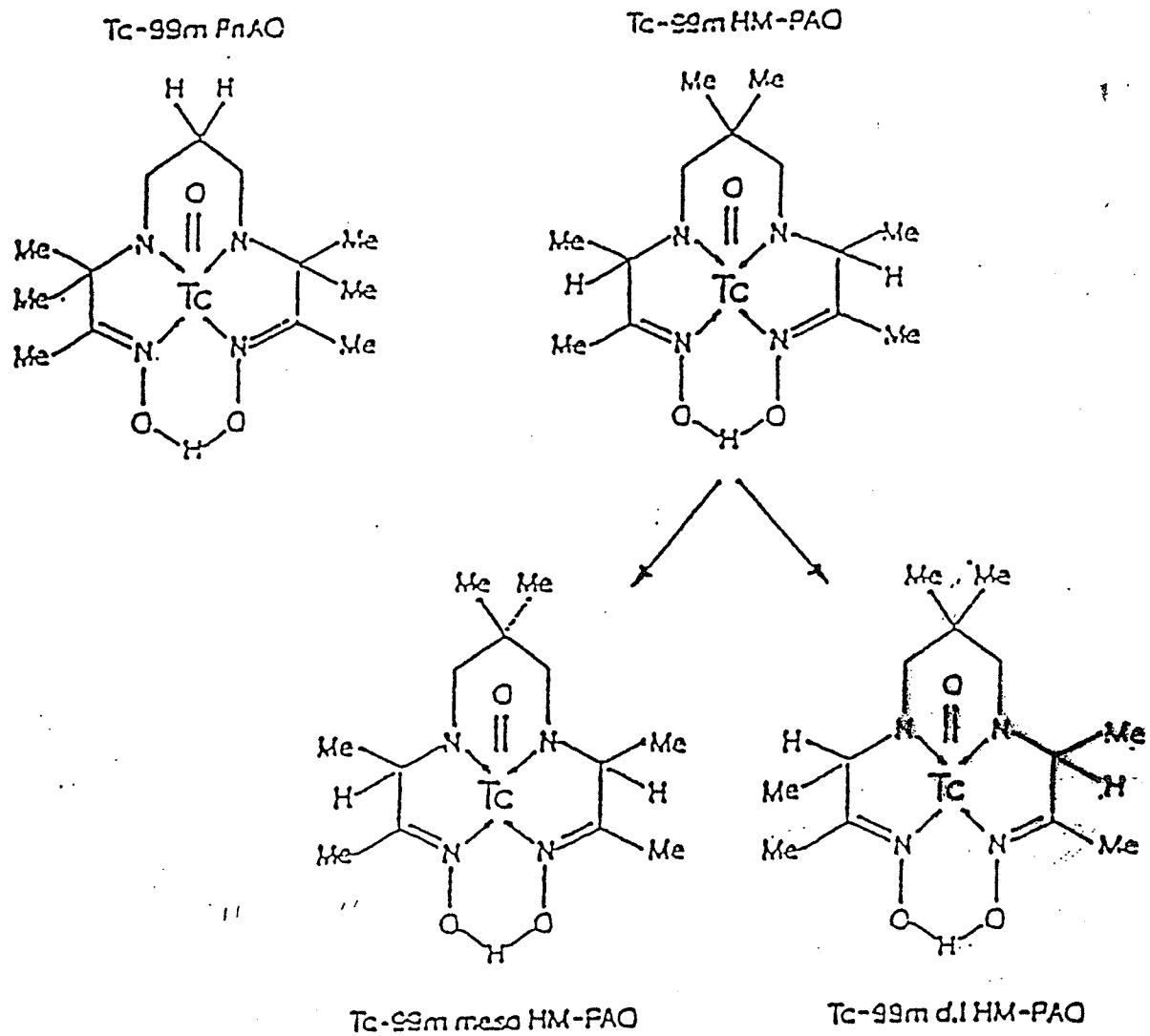


Fig 1.6 : Tc-99m complexes of PnAO and HMPAO [Eil, 1985].

Chapter 2

Compartmental Analysis

2.1. Introduction

The aim of compartmental analysis is to construct a mathematical model of a certain type of physical system, which is sufficiently general to apply in a wide range of experimental conditions. This chapter consists of two main sections. The first section introduces the theory of compartmental systems, including the basic terms and the general assumptions which are taken into account. Secondly, this chapter deals with the use of computers in compartmental analysis. In particular, a computer package called *SAAM* (Simulation, Analysis, and Modeling) will be described.

2.2. Compartmental Systems

A compartmental system is one which is made up of a finite number of macroscopic subsystems, called compartments. Each compartment is homogeneous and well-mixed, and the compartments interact by exchanging material. Because the interactions between compartments include the transfer of material (mass) some type of mass conservation condition holds for all transfers between compartments, and between compartments and the external environment. If there is no exchange between the compartments and the environment the system is said to be closed, otherwise if there is exchange between compartments and the environment the system is said to be open. The

mathematical theory of such compartmental systems is called compartmental analysis [Jacquez, 1988]. In other words, compartmental analysis is a physical description of the mathematical equations that define the transfer of material between the compartments.

The application of compartmental analysis can be considered in terms of three main problems [Robertson, 1957]. The first problem is the development of an acceptable model for any particular biological system. This requires considerable background knowledge of the field from which the problem arises. This knowledge should provide some justification for the use of a compartmental model, while the structure and parameters of the model should have meaning in terms of known processes and the structure of the real system. Otherwise a compartmental system description may be of little relevance to the real world. Secondly, in a specific compartmental model, there is the problem of developing the analytic theory for such a system. This is a problem in mathematics and is usually the best defined, if not the easiest, of the three. The third, and usually most difficult, problem is the so-called "inverse problem", which involves selection of the best model from several plausible models, and identifying the data which must be collected to substantiate the model.

In the following sections the basic terms and assumptions involved in compartmental analysis will be discussed.

2.2.1. Tracers

In most nuclear medicine studies, a tracer is a labeled form of a substance. Ideally, the label makes the labeled form detectable by the observer without affecting its behavior in the system being studied. In general, the purpose of a tracer experiment is to deduce certain properties of the system being studied from observations of the behavior of the tracer when it is introduced to the system. In particular, the distribution

kinetics of tracers provide a basis for determining the volumes or masses of components of the system and the rate of transfer of substances among these components.

In many instances [Wartak, 1983] an isotope of one element has been considered as a substitute tracer for a chemically similar element. Other substances, such as inert gasses not normally present in the system being studied, may sometimes be used as tracers also. In nuclear medicine over 90% of all, *in-vivo*, studies are carried out by radiopharmaceuticals (tracers) labeled with $Tc-99m$ [Eli, 1987]. The tracer *HMPAO* labeled with $Tc-99m$ is used in our study of regional cerebral blood flow (*rCBF*), and will be discussed in chapter three.

2.2.2. Compartments

Pharmacokinetic analysis of tracer disposition in the human body is based on several assumptions. The principal assumption is that the human body may be represented by one or more compartments or pools in which the tracer resides in a dynamic state for a period of time.

A compartment is an amount of material that acts kinetically like a distinct, homogeneous amount of material. It is to be distinguished from a physical volume or physiological space [Robertson, 1983].

The size and volume of each compartment are assumed to remain constant. Therefore, any equation describing the time course of the amount of tracer in a given compartment can be converted to an equation describing the time course of concentration of the tracer in that compartment by dividing both sides of the equation by the volume of the compartment.

A consequence of the assumption that each compartment is well mixed is that a tracer entering the compartment is instantaneously and uniformly distributed throughout the entire compartment. Thus, the tracer concentration in a certain region of

the compartment is the same as the tracer concentration of the entire compartment.

As mentioned earlier, in many models the tracer not only transfers from one compartment to another, but also exchanges with the outside world as well. Such systems are called open systems. So called closed systems do not communicate with the outside world.

Since activity is removed from the system comprising the brain tissue and its blood supply, the open system was therefore selected in this study.

2.3. Use of Computers in Compartmental Analysis

In the study of biological systems, a model is usually selected to describe the system under study. The model can be chosen in such a way that it can be formalized in mathematical language and used for further prediction or simulation. Analytic solutions, if possible, are often very tedious. However, using appropriate software, computers can be used to solve numerically the equations of a given model. As a result, the researcher can concentrate on the development of a suitable model rather than the analytical mathematics.

Once the model has been chosen, computer simulations can be performed to analyze the developed differential equations using the selected software. Such programs usually contain an input subroutine that instructs the computer to accept initial conditions, and an output subroutine that instructs the computer to print out the results in a form which is readily interpreted. Figure 2.1 shows a flowchart of such a program.

The input subroutine usually contains instructions that request the user to choose the desired model (one compartment, two compartment, etc.), to select a particular schedule and method of administration of radioactivity or other tracer, and to specify the initial values for a given simulation. On the other hand, the output subroutine contains instructions that present the results of the analysis and associated error data. The simulation itself is performed by a sequence of instructions that substitutes the data supplied by the input subroutine for various constants and variables in the differential equations and solves them for a specified number of successive time samples.

Pharmacokinetic analysis based on curve fitting is best carried out by means of non-linear estimation programs such as *BMDP* [Garcia, 1979], *NONLIN* [Metzler, 1974], Worsley [1960], and *SAAM* [Berman, 1974], which were designed for use with several different computers.

The *SAAM* software became more popular as an all purpose program to study typical radiotracer problems using compartmental modelling. This software was also

available on our AMDAHL mainframe computer at the University of Manitoba and was used through the course of this research work.

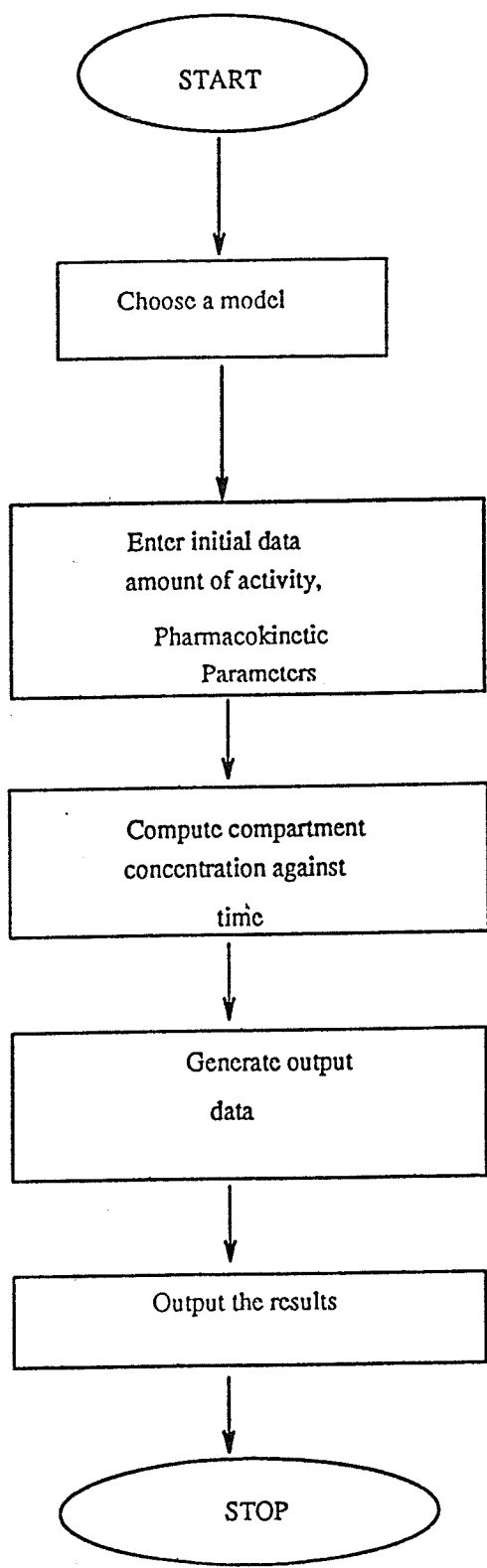


Fig. 2.1 : Flow chart of a program to simulate kinetic behavior of tracers [Wartak, 1983].

2.3.1. Computer Simulation Utilizing the SAAM Package

SAAM (Simulation, Analysis, and Modeling) is a single, general purpose computer program developed for the analysis of data within the context of a proposed model. It can perform simulation, i.e., solve a set of user-defined equations to study the biological implications of the model, or analyze and model by fitting experimental data to defined parametric functions. The equations describing the model may be differential, integral or algebraic, the only restriction being that an analytical or numerical procedure must exist for their solution.

The computational structure of *SAAM* can be classified into four stages [Robertson, 1983]. The first stage is solving the set of differential equations, by numerical techniques. The method of Runge-Kutta [Levy, 1950] is used in *SAAM* to solve the developed differential equations, for a set of initial conditions. The second stage is the comparison of the generated results with the available experimental data. This is achieved by means of the sum of the squares of the differences between the experimental data and that generated from the assumed initial conditions. The third stage is the iterative adjustment of the initial parameters to minimize the sum of the squares of the deviations. This can involve both linear and non linear data fitting procedures. Deriving statistical information is the fourth stage. This involves approximations to give estimates of the uncertainties of the fitted parameters, and the listing and plotting of both experimental and calculated data.

Programs like *SAAM* are useful because, firstly, the users do not require a detailed understanding of the mathematics, and secondly, alterations in the model formulated are easily executed. Also such programs can be formulated in terms of biologically significant parameters, unlike standard mathematical curve fitting routines which require the user to interpret their output. The main difficulty with *SAAM* and simulation programs, in general is providing realistic initial estimates of the parameter values.

A user manual for *SAAM* is written so that a researcher can define a specific compartmental model and enter the parameters or the data to be fitted directly into this model. To run *SAAM*, the user must create a *SAAM* input listing. This is a coded statement of the modeling problem, which *SAAM* can interpret. When successfully run, a *SAAM* deck produces an output that contains plots of the predicted and observed values, statistical information, and information on convergence if non-linear parameters are being adjusted. The *SAAM* code language is given in Berman, [1974].

Chapter 3

Compartmental modeling

3.1. Introduction

In this chapter the development of a four compartmental model of the brain and the distribution of $Tc-99m-HMPAO$ within the four compartments is introduced. Four coupled differential equations which mathematically describe the physical nature of the blood flow in the brain are presented. The proposed model is compared with other existing mathematical formulations in the literature.

3.2. The Concept of the Extraction Fraction, (E)

In most tissues, an injected bolus traversing the capillary bed can be divided into two fractions [Lassen, 1981]. First is the extracted fraction E which diffuses through the membrane, distributes outside the capillary, and then diffuses back to be cleared by capillary blood. Second is the non extracted or transmitted fraction $(1-E)$ which does not cross the capillary membrane.

To describe the capillary membrane and transport of the tracer in physical terms, it is convenient to take as a basic assumption that the capillaries in an organ are similar with respect to length, surface area and blood flow. Data from whole organ studies are, therefore, essentially based on what has been called the "single capillary" model [Kety, 1951].

Consider a single capillary as shown in Fig. 3.1. Assume the tissue concentration remains relatively constant at some mean value C_i during passage of the blood from the arterial to venous end of the capillary. Also it is assumed that the blood flow is in the x cartesian coordinate direction and that diffusion is perpendicular to the flow, i.e., y direction. Let,

S' = the diffusion surface area per unit length of capillary,

V = the volume per unit length of capillary,

$C_b(x)$ = concentration of tracer in blood,

x = coordinate measured along length of capillary,

λ = partition coefficient, i.e., ratio of equilibrium concentration of a tracer in the tissue to that of blood.

From Fig 3.1, the tracer concentration in the capillary wall immediately adjacent to the lumen (1) is equal to $\lambda_1 C_b(x)$, where λ_1 is the ratio of concentration in wall to the concentration in blood. Also, the capillary wall concentration adjacent to the tissue (2) is $\lambda_2 C_i$, where λ_2 is the ratio of concentration in the wall to that in tissue. The partition coefficient, λ , may be defined by:

$$\lambda = \frac{\lambda_1}{\lambda_2} = \frac{C_i}{C_b(x)} \quad (3.1)$$

One can apply Fick's diffusion law, given below, to capillary diffusion:

$$\frac{dq}{dt} = -DS \frac{\partial C}{\partial x} \quad (3.2)$$

where, S is the surface area, and D is the diffusion constant with the unit of $\frac{cm^2}{sec}$, which relates the amount of substance dq diffusing in time dt across area S to the concentration gradient.

From Fig. 3.1, and application of Fick's law, given by equation (3.2), one can obtain the following relations,

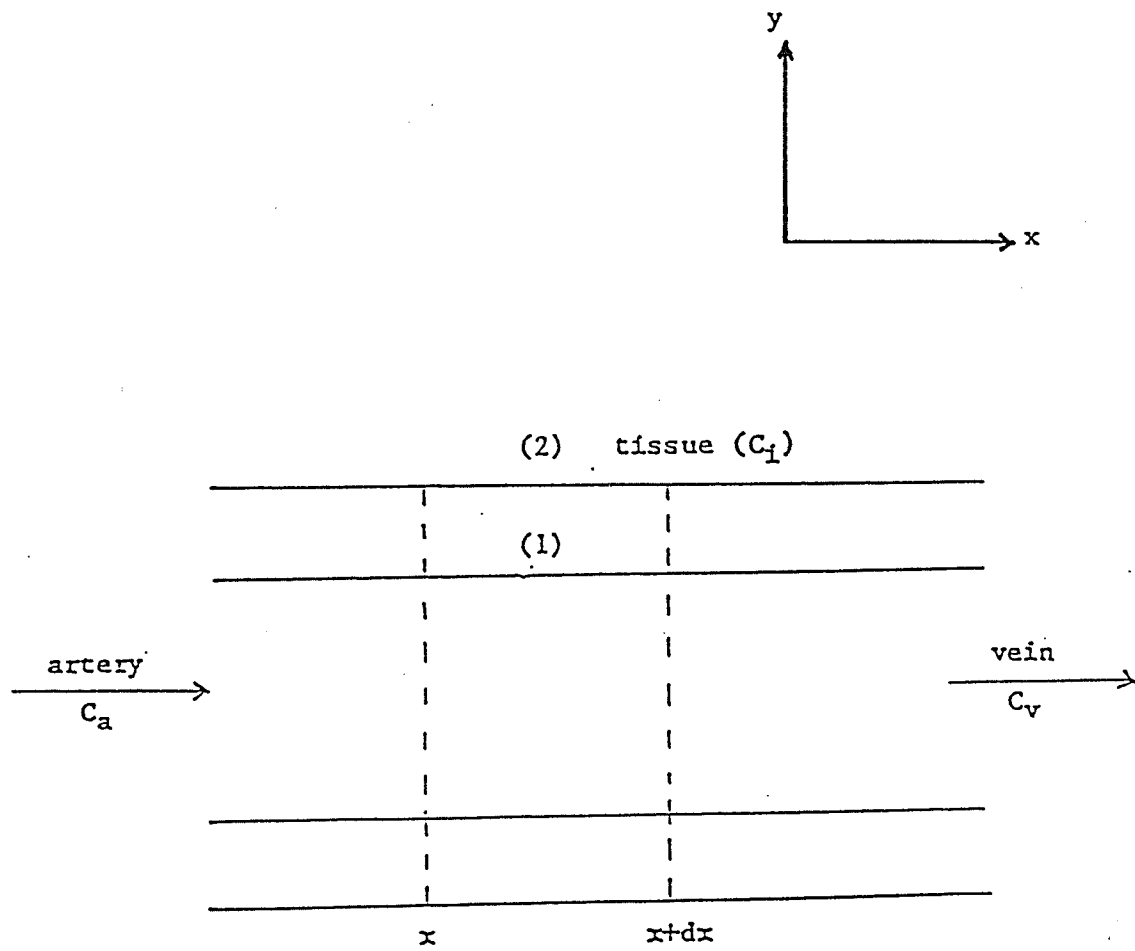


Fig. 3.1 : Diagram of a single capillary [Kety, 1951].

$$\frac{dQ_b}{dt} = -DS' dx \frac{C_1 - C_2}{H} \quad (3.3)$$

where Q_b is the amount of the tracer in blood, $C_1 = \lambda_1 C_b(x)$, is the concentration of tracer in capillary wall on lumen side, $C_2 = \lambda_2 C_i$, is the concentration of tracer in capillary wall on the tissue side, and H is the capillary wall thickness. With substitution of equation (3.1) in (3.3), one obtains,

$$\frac{dQ_b}{dt} = - \frac{DS' dx}{H} [\lambda_1 C_b(x) - \lambda_2 C_i] \quad (3.4)$$

The permeability of the capillary wall, P , is defined as,

$$P = \frac{D}{H} \lambda_1 \quad (3.5)$$

which can be substituted in (3.4) to yield,

$$\frac{dQ_b}{dt} = - S'P [C_b(x) - \frac{C_i}{\lambda}] dx \quad (3.6)$$

Next, considering just the blood, and the relation $C = \frac{Q}{V}$, over an elemental capillary length, one can relate the tracer concentration to the blood flow as below,

$$\frac{dQ_b(x)}{dt} = V \frac{dC_b(x)}{dt} \quad (3.7)$$

But, $F = \frac{V}{dt}$, where F is the blood flow. So,

$$\frac{dQ_b(x)}{dt} = F dC_b(x) \quad (3.8)$$

From equation (3.6) and (3.8),

$$- S'P [C_b(x) - \frac{C_i}{\lambda}] dx = F dC_b(x) \quad (3.9)$$

and rearranging (3.9),

$$\frac{dC_b(x)}{dx} = -\frac{S'P}{F} \left[C_b(x) - \frac{C_i}{\lambda} \right] \quad (3.10)$$

Since C_i and λ are independent of x , i.e., $\frac{d}{dx} \left(\frac{C_i}{\lambda} \right) = 0$, the term $-\frac{C_i}{\lambda}$ may be added to the left hand side of (3.10), giving:

$$\frac{d}{dx} \left[C_b(x) - \frac{C_i}{\lambda} \right] = -\frac{S'P}{F} \left[C_b(x) - \frac{C_i}{\lambda} \right] \quad (3.11)$$

which has the solution given by,

$$C_b(x) - \frac{C_i}{\lambda} = A e^{\left(\frac{-S'Px}{F}\right)} \quad (3.12)$$

where A is the normalization constant which can be obtained by applying the boundary condition at $x = 0$, i.e., equating the arterial concentration, C_a , to that of concentration of tracer in blood, C_b , evaluated at $x = 0$. That is,

$$x = 0, \quad C_b(0) = C_a \quad \text{the arterial concentration}$$

and,

$$A = C_a - \frac{C_i}{\lambda}$$

which results in an equation of the form,

$$C_b(x) - \frac{C_i}{\lambda} = \left[C_a - \frac{C_i}{\lambda} \right] e^{\left(\frac{-S'Px}{F}\right)} \quad (3.13)$$

Similarly, at

$$x = L, \quad C_b(L) = C_v$$

where L is the capillary length, and C_v is the venous concentration. Defining the total capillary surface area as $S'L = S$, the solution takes the form of,

$$C_v - \frac{C_i}{\lambda} = \left[C_a - \frac{C_i}{\lambda} \right] e^{\left(\frac{-PSL}{F}\right)} = \left[C_a - \frac{C_i}{\lambda} \right] e^{\left(\frac{-PS}{F}\right)} \quad (3.14)$$

Subtraction of C_a from both sides of (3.14), yields the following equation,

$$-C_a + C_v - \frac{C_i}{\lambda} = -C_a + C_a e^{\left(\frac{-PS}{F}\right)} - \frac{C_i}{\lambda} e^{\left(\frac{-PS}{F}\right)} \quad (3.15)$$

After further manipulation, (3.15) takes the form of

$$C_a - C_v = \left[C_a - \frac{C_i}{\lambda} \right] \left[1 - e^{\frac{-PS}{F}} \right] \quad (3.16)$$

Since $F(C_a - C_v)$ is equal to the amount of tracer lost from the capillary in a single pass of tracer through the capillaries, and $F\left(C_a - \frac{C_i}{\lambda}\right)$ is the amount of tracer transferred to the tissue region by blood flow in a single pass then, by definition

$$E_i = \frac{C_a - C_v}{C_a - \frac{C_i}{\lambda}} \quad (3.17)$$

is the extraction efficiency, E_i , of the tracer. The extraction efficiency at any instant however is related to the permeability coefficient P [Crone, 1963]. Therefore, equation (3.16) can be written in terms of E_i as,

$$E_i = 1 - e^{\left(\frac{-PS}{F}\right)} \quad (3.18)$$

The derivation of (3.18) was based on the assumption that there is a net outward diffusion proportional to the intravascular concentration at any place along the capillary, i.e., that the intravascular concentration falls exponentially or almost exponentially [Crone, 1963]. It should also be noted that the extraction efficiency as defined by equation (3.17) takes the back diffusion (from tissue into blood) into account. In the special case where there is no back diffusion of tracer from tissue to blood, equation (3.17) reduces to

$$E_i = \frac{C_a - C_v}{C_a}$$

This is the form used by Mintun [1984] in their formulation of oxygen utilization in tissue. The extraction efficiency as defined by equation (3.18) was therefore used in the analysis of $rCBF$ in this research work as it will be further discussed in the following section.

3.3. A Four Compartmental Model of The Brain

The measurement of $rCBF$ has been pursued by methods generally based on kinetic models that require the administration of tracer substances and the measurement of their concentration in arterial blood and brain tissue [Kety, 1951]. The use of radioactive substances has allowed the *in-vivo* assay of the local concentration of tracer in tissue. In the past decade the measurement of local tissue concentrations of gamma-emitting radioactive tracers by *SPECT* has been investigated as a possible tool to determine $rCBF$ following the administration of radioisotopes [Matsuda, 1988]. However, the measurement of radioactivity distribution does not provide any information on the physiology or biochemistry of the brain or system under study unless it is combined with kinetic models of tracer distribution in arterial blood and brain tissue. For this reason the selection of a proper tracer, of the timing of the procedure, and the system used for the recording of the radioactivity are of critical importance to obtain meaningful information on brain physiology [Lucignami, 1985].

To analyze the *in-vivo* kinetic behavior of $Tc-99m-HMPAO$, we used a kinetic model consisting of four compartments and four rate constants. Selection of four compartments was based on the distribution of $Tc-99m-HMPAO$ in blood and the brain tissue. Since $Tc-99m-HMPAO$ has a lipophilic form which undergoes conversion to non-diffusible hydrophilic components in both blood and brain tissue, a four compartment model is required to describe its distribution. Fig. 3.2, describes the developed model schematically. In the figure, the top two compartments represent the tissue compartments and the bottom two represent the blood compartments. Dividing the model vertically, the two lipophilic compartments of $Tc-99m-HMPAO$ are on the left, and the hydrophilic compartments of $Tc-99m-HMPAO$ are on the right.

In this model, compartment one represents the lipophilic diffusible tracer in the arterial blood and compartment two represents the lipophilic diffusible tracer inside the brain tissue. Compartment three represents the hydrophilic non-diffusible tracer that is

trapped in the brain tissue and compartment four represents the non-diffusible tracer trapped in the blood. The triangle in the center of the figure is a "summer" compartment [Berman, 1974] which reflects the sum of the activities in all four compartments. Since each compartment by itself is not a physical volume, it is not possible to see each compartment separately on a *SPECT* image, nor it is possible to measure the activity of each compartment separately. The summer compartment is used as a constraint on the fitting of parameters to experimental data, but plays no part in the transfer of the tracer between the other four compartments.

The appropriate differential equations for this system are the following:

$$\begin{aligned} \frac{dq(1)}{dt} = & -L(2,1)q(1) + L(1,2)q(2) + UF(1) \\ & - L(4,1)q(1) - L(0,1)q(1) \end{aligned} \quad (3.19)$$

$$\frac{dq(2)}{dt} = L(2,1)q(1) - L(1,2)q(2) - L(3,2)q(2) \quad (3.20)$$

$$\frac{dq(3)}{dt} = L(3,2)q(2) \quad (3.21)$$

$$\frac{dq(4)}{dt} = UF(4) + L(4,1)q(1) - L(0,4)q(4) \quad (3.22)$$

where $L(2, 1)$, $L(1, 2)$, $L(3, 2)$, and $L(4, 1)$ represent the rate constants between the four compartments, $L(0, 1)$, and $L(0, 4)$, are the rate constants of the tracer in the blood leaving the system, the q 's are the quantity of tracer in each compartment and $UF(1)$ and $UF(4)$ are the input functions defined as,

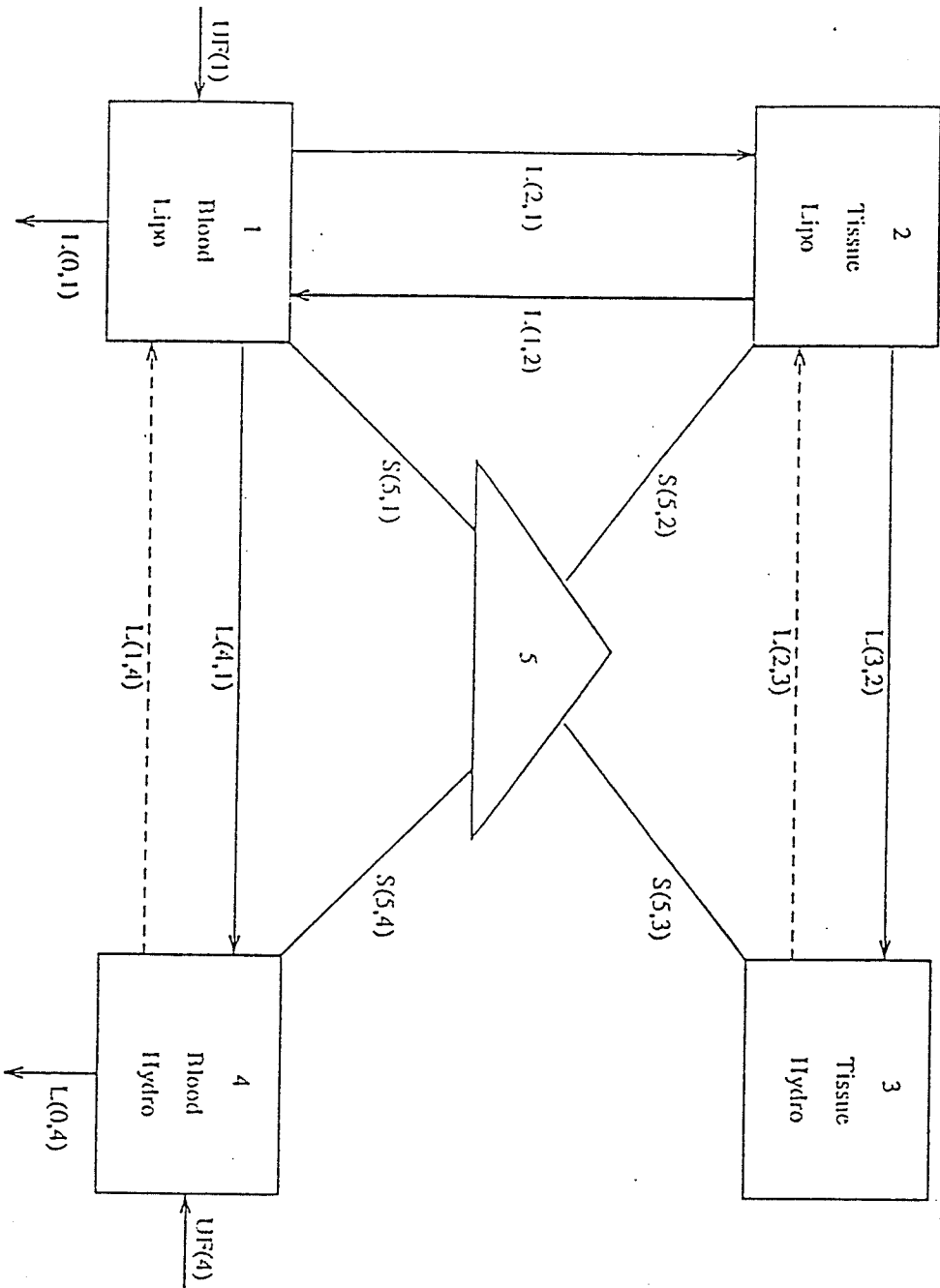


Fig. 3.2 : A four compartmental model of the brain.

$$UF(1) = t^2 e^{-2t} e^{-0.5t} \quad (3.23)$$

$$UF(4) = t^2 e^{-2t} (1 - e^{-0.5t}) \quad (3.24)$$

where $t^2 e^{-2t}$ defines the total activity [Lee, 1988], and the exponential term $e^{-0.5t}$ defines the fraction of lipophilic tracer in blood. Equations (3.23) and (3.24) are defined under the assumption that the blood samples are taken from the carotid artery. For the purpose of the model it is also assumed that conversion of the lipophilic compartment to the hydrophilic compartment commences at time zero. Clearly this is an approximate since it is known that conversion of up to about 12% will occur giving 88% [Andersen, 1988] lipophilic component in vitro before injection.

The above differential equations were obtained based on the assumption that the trapping of $Tc-99m-HMPAO$ is irreversible, i.e., $L(2,3) = L(1,4) = 0$. The dotted lines in Fig. 3.3 signify this irreversible trapping. The trapping mechanism of $Tc-99m-HMPAO$ in brain tissue is thought to be caused by conversion to a hydrophilic complex, possibly by opening of the bond between the oxime groups [Neirinckx, 1986]. After passage of the lipophilic $Tc-99m-HMPAO$ through the *BBB* the hydrophilic component is trapped inside the brain tissue. This conversion is accelerated by certain proteins [Neirinckx, 1986]. The other assumption is that there is no passage of the non-diffusible form of the tracer across the blood-brain-barrier, i.e., no exchange between compartments three and four [Matsuda, 1988]. $L(2,1)$ and $L(1,2)$ describe the transport of $Tc-99m-HMPAO$ between the tissue and blood. The clearance of lipophilic material from blood to tissue is given by,

$$L(2,1) = FE \quad (3.25)$$

where F is the flow and E is the extraction efficiency, defined by Crone's equation as

$$E = 1 - e^{-\left(\frac{PS}{F}\right)} \quad (3.26)$$

where PS is the product of the permeability and the surface area. $L(1,2)$, describes

the washout of lipophilic complex from tissue to blood. For a freely diffusible complex such as $Tc-99m-HMPAO$ [Lassen, 1987],

$$L(1,2) = \rho L(2,1) = \rho FE \quad (3.27)$$

where ρ is the density of the tissue.

For the lipophilic $Tc-99m-HMPAO$ complex, the rate of trapping is described by $L(3,2)$. The fraction of agent trapped, R , is defined by,

$$R = \frac{L(3,2)}{L(3,2) + L(1,2)} \quad (3.28)$$

The fraction retained in the human brain has been determined by Andersen [1988], using a technique involving intra-carotid injection of $Tc-99m-HMPAO$ and analysis of the first pass brain wash-out curve. The value thus obtained for R is 0.60. Therefore, knowing the fraction of agent trapped and the washout of lipophilic complex from tissue to blood, i.e., $L(1,2)$, $L(3,2)$ can be calculated.

The same approach could be used to calculate the rate of trapping in the blood, $L(4,1)$,

$$R' = \frac{L(4,1)}{L(4,1) + L(2,1)} \quad (3.29)$$

3.4. Related Works on The Measurement of CBF using Compartmental Models

Since the introduction of $Tc-99m-HMPAO$, many compartmental models have been proposed to describe the transport of this tracer in the brain. In this section some of these techniques are discussed.

Matsuda [1988] developed a kinetic model for quantitating CBF using $Tc-99m-HMPAO$. The model is shown in Fig. 3.3, and is based on the work of Lassen [1987]. The values for the flow and rate constants for the kinetic model of $Tc-99m-HMPAO$ distribution in the human brain were determined. Time course data of brain activity and arterial blood activity of the tracer were fitted to the four compartmental model. Similar to our model, the first compartment is the diffusible tracer in the arterial blood at concentration Ca_D . The second compartment is the nondiffusible tracer that is trapped in the blood at concentration Ca_{ND} . The third compartment is the lipophilic diffusible tracer inside the brain tissue at concentration Cb_D and the fourth compartment is the hydrophilic nondiffusible tracer that is trapped in the brain tissue at concentration Cb_{ND} . The rate constants, Ls , define the transport of the tracer between compartments. The single pass extraction efficiency of $Tc-99m-HMPAO$ was determined in the rat brain by the indicator diffusion method [Crone, 1963]. The value of the extraction efficiency, E , was then assumed to be constant throughout the brain. As a simplification, the arterial curve for lipophilic tracer was not actually determined in his study, but a simple mono-exponential decrease in radiochemical purity was assumed to account for the rapid conversion of $Tc-99m-HMPAO$ from the lipophilic to a hydrophilic compound in the blood.

Next, a set of differential equations between compartments were obtained by assuming that the trapping was irreversible and there was no passage of the non-diffusible form of the tracer across the blood-brain-barrier. A convolution integral over time of these differential equations was developed to relate the total brain tissue

concentration, $C_b(t)$, to the time taken to scan the brain.

The determination of flow and the rate constants in the human brain of four patients with various cerebrovascular disorders were based on the developed convolution integral equation. First, the total brain tissue concentration of the tracer $C_b(t)$ was determined by repeatedly scanning at one level over a period of 30 minutes after the intravenous injection of $Tc-99m-HMPAO$. Next, the arterial blood concentration $C_a(t)$ was obtained by sampling arterial blood and fitting to a cubic spline approximation. The values of the rate constants were obtained by fitting the time course data of $C_b(t)$ and $C_a(t)$ to the developed convolution integral. Values of blood flow and the rate constants for back diffusion of the diffusible tracer from brain to blood, $L(1, 3)$, conversion of the lipophilic tracer to the nondiffusible form in the brain, $L(3, 4)$, and conversion of the diffusible tracer to the nondiffusible form in blood, $L(2, 1)$ were determined.

It should be noted that our developed compartmental model is similar to that of Matsuda's model, but differs in the form of the arterial input functions and the fact that no convolution integral was included. The same assumptions were made for irreversible trapping and constant extraction efficiency. However, as pointed out by Matsuda [1988] the assumption of constant E is valid only from a practical point of view, and the potential for a variance of E should be recognized. Matsuda's [1988] procedure involved a convolution integral of the differential equations to obtain values of blood flow and the rate constants. However, the developed differential equations in the present study were solved directly using computer simulations. Also, Matsuda [1988] observed that the diffusible tracer rapidly decreases in the blood and approaches zero by two minutes after injection. This was also evident in our observations, as will be discussed in the following chapter.

Lassen [1988] presented a kinetic analysis of the uptake and retention of $Tc-99m-HMPAO$ in the human brain. He used a technically simpler approach than

that of Matsuda [1988]. It is based on the brain's response to a unit impulse input implemented as a bolus injection of $Tc-99m-HMPAO$ into the internal carotid artery in humans. The bolus injection insures a compact arrival of the tracer in the brain vessels. His model [Lassen, 1988] was based on three compartments: the lipophilic tracer in the blood pool of the brain, the lipophilic tracer inside the brain, and the hydrophilic form retained in the brain. The hydrophilic part of the tracer in the blood was not included in his model. Cerebral blood flow, F , was measured using the $Xe-133$ intra-carotid injection method [Lassen, 1988]. $Xe-133$ is the gold standard tracer for the clinical evaluation of flow to the brain, and is often used in studies of $rCBF$. The extraction efficiency, E , of $Tc-99m-HMPAO$ was then calculated from the measured flow value using the empiric regression equation that was derived in studies in human brain by Andersen [1988]. Since Lassen's work [1988], was mainly concentrated on the brain tissue, he did not introduce the fourth compartment, for the distribution of hydrophilic $Tc-99m-HMPAO$ in blood, therefore the rate of trapping in blood was given a value of zero. Therefore this resulted in a simpler model.

The kinetic behavior of $Tc-99m-HMPAO$ in human brain in eleven patients with various brain diseases was also studied by Murase [1992] using *SPECT*. The developed model was based on four compartments with five parameters. These parameters were defined as the rate constant for the transport of $Tc-99m-HMPAO$ from blood to brain, back diffusion from brain to blood, conversion to a hydrophilic form in the brain, conversion to a nondiffusible form in the blood, and the fraction of radioactivity attributable to the vascular compartment. Similarly he assumed that the trapping of $Tc-99m-HMPAO$ was irreversible and that the non-diffusible form of the tracer did not cross the blood-brain-barrier. A set of differential equations for the kinetic model were developed, and their solution obtained via a convolution integral to again account for the imaging time. To solve the convolution integral numerically a recursive relation [Mazoyer, 1986] was introduced to reduce the calculation time without

sacrificing accuracy. To estimate the rate constants, the integral equation was fitted to the time course data of brain activity measured by dynamic *SPECT* using the non-linear least-squares method [Beck, 1977].

Using this kinetic model and dynamic *SPECT*, Murase [1992] investigated the behavior of $Tc-99m-HMPAO$ tracer in the human brain and the possibility of using it to quantitate *CBF*. A good fit was obtained between the model predictions and the dynamic scan data, suggesting the validity and utility of the model.

As discussed above, Matsuda [1988] used a four compartmental model with four parameters. Whilst, Murase [1992] used a four compartment five parameter model. The model of Murase [1992] provided the better fit between the model and the dynamic scan data, implying that the vascular compartment can not be neglected in the kinetic model. The much shorter convolution interval of the Murase [1992] model (40sec/scan) and the arterial blood sampling would contribute to the better accuracy of the model.

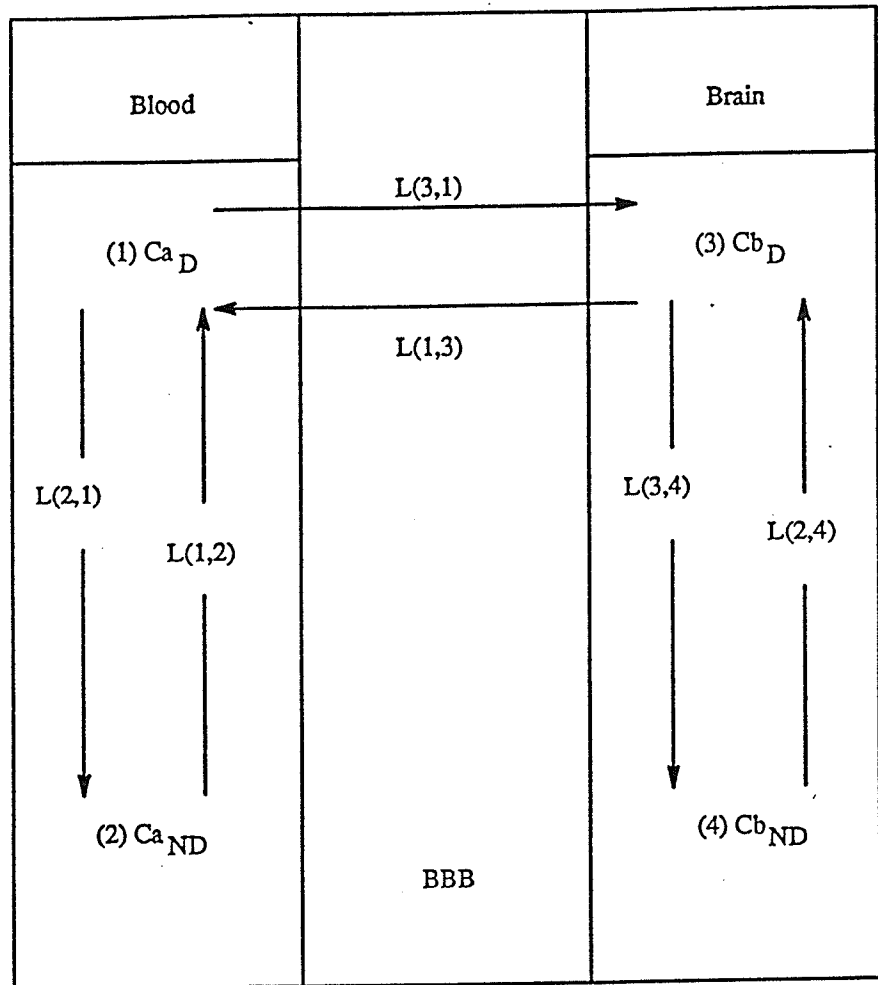


Fig. 3.3 : Diagrammatic representation of the kinetic model for determining cerebral blood flow and the rate constants using $Tc-99m-HMPAO$ [Matsuda, 1988].

3.5. Summary

In summary, a four compartmental model has been developed to describe the transport of $Tc-99m-HMPAO$ to the brain tissue. The related works of Matsuda [1988], Lassen [1988], and Murase [1992], were discussed and a descriptive comparison among them was made and presented in the last section. The three compartmental model introduced by Lassen [1988] did not include the hydrophilic component of the tracer in blood. This resulted in a simpler model, but, information on the conversion rate in blood was not obtained.

Unlike Lassen [1988], Matsuda [1988] introduced a quantitative approach using a model which took both blood and brain tracer kinetics into account. Kinetic parameters were obtained from a multiparametric fitting to a four compartment model based on multiple *SPECT* image acquisition as well as arterial radioactivity samples. He applied the model to determine flow and rate constants in human brain in four patients with various cerebrovascular disorders. Similar to our model, Matsuda [1988] assumed that the single pass extraction efficiency, E , for transport of $Tc-99m-HMPAO$ is constant throughout the brain and independent of flow. However, Matsuda [1988] observed that the diffusible tracer rapidly decreases in the blood and approaches zero by two minutes after injection. In other words, the input function to the brain was negligible after two minutes and independent of the arterial blood radioactivity thereafter. Similar behavior was also observed on the time activity curve in our compartmental model as will be discussed in the following chapter.

Recently, Murase [1992] reported a four compartmental model with five parameters to study the transport of $Tc-99m-HMPAO$ in eleven patients with brain diseases. His model included the effect of radioactivity attributable to the vascular compartment, which could not be neglected in the kinetic model. However, as discussed earlier this model requires fast dynamic *SPECT* data acquisition and arterial blood sampling.

It should be mentioned that although Lassen [1988], Matsuda [1988], and Murase [1992] have applied their models experimentally, none of these studies include the determination of the input arterial concentration of lipophilic $Tc-99m-HMPAO$ to the brain. The major limitation in assessing arterial input functions has been identified as the isolation of the circulating radioactive tracer (diffusible) from its non-*BBB* crossing radioactive conversion products (non-diffusible) [Andersen, 1988].

Conversely, in our work the analysis of cerebral blood flow was performed through computer simulations. Furthermore, the differential equations developed in our model, also included outflow, $L(0, 1)$, $L(0, 4)$, and the input functions, $UF(1)$, $UF(4)$ which were not present in the work presented by other researchers. Finally, the aim and emphasis of this thesis is to study the effect of noise on the blood flow. Therefore, rather than using the convolution technique with its additional parameters and experimental complexity, the differential equations were solved directly and multiple simulations used to study the variability, or noise, in the blood flow. The details of the computer simulations are described in the next chapter.

Chapter 4

Methods and Results

4.1. Introduction

This chapter deals with experimental procedures and the results of the computer simulation of the compartmental model introduced in the earlier chapters (model shown in Fig. 3.2). To carry out the simulation a computer package called *SAAM* (Simulation, Analysis, and Modeling) [Berman, 1974] was used as mentioned earlier.

4.2. Experimental Procedures

The experiments were based on computer simulations and can be summarized as follows.

4.2.1. Noise Free Experiments

The first step in these experiments was to simulate the $Tc-99m-HMPAO$ distribution between blood and tissues in the brain. To carry out the calculations, a set of input parameters was assumed. The values of these input parameters (Table 4.1), i.e., extraction efficiency [Lee, 1988], tissue density, permeability surface area product, the fraction of agent trapped, and the initial values for the rate constants were all obtained

through a literature search [Andersen, 1986]. Using these parameters and the four compartment model, a time activity curve was calculated for each compartment. These four curves were summed to generate the "total time activity curve" of the "summer" compartment, number five. Each of these five curves was stored as a discrete set of x-y coordinates, not as a functional relationship.

The second step in these noise free experiments was to select only a finite number (10) of points evenly distributed over the first 10 minutes of the total time activity curve (summer compartment five) together with the arterial distribution functions, to fit the model to this "experimental" data, and to calculate the rate constants and other parameters of the model. Clearly, the fit is expected to retrieve those parameters used as input to the first step defined above.

The purpose of these experiments was to verify that both operational modes of SAAM, generation of "experimental" curves from parameters, and calculation of parameters by fitting to curves, were operating correctly. Also, the variation of a specific parameter with another was investigated whilst holding the rest constant. The details of these experiments are given in section 4.3.

4.2.2. Experiments with Added noise

These experiments again used the total time activity curve of compartment five and the functional arterial activity curves to calculate the rate constants and blood flow. The difference between these experiments and those detailed above was that each of the 10 points of the total activity curve was modified by addition of Gaussian noise [Papoulis, 1965] prior to application of the non-linear least squares regression analysis. To study the effect of noise on the precision and accuracy of the rate constants and hence $rCBF$ determination, various amount of Gaussian noise were added to the theoretical total time activity curve and many simulations made at each noise level.

The details of these experiments are given in section 4.4.

4.3. Calculation of the Rate Constants and Flow with no Error Added

This section presents the results of computer simulations which were conducted to study the developed compartmental model of $Tc-99m-HMPAO$. At this stage simulations were performed without the presence of noise. The initial input values for the rate constants and blood flow (Table 4.2) obtained from the literature were used to generate the total time activity curve consisting of 20 points over a period of 10 minutes, at 0.5 minute time intervals. The simulation was then further divided into three stages.

The first stage was generation of an input file. Fixed parameters such as extraction efficiency, tissue density, permeability surface area, and the fraction of agent trapped as well as the previously generated total time activity curve were recorded in the input file called *SAMDAT*. Table 4.1 lists the values of these parameters that were used in the computations. These parameters describe the characteristics of the patient and the radiopharmaceutical $Tc-99m-HMPAO$ [Andesen, 1986].

The second stage was to solve the differential equations of the compartmental model given in (3.19) through (3.24) by curve fitting, using the input parameters listed in table 4.1 and the total time activity curve. The procedure for modelling differential equations is fully described in the *SAAM* manual [Berman, 1974]. The same format was adopted here, accordingly.

The final stage was the output of the generated quantities, i.e., blood flow and the rate constants. These results are listed in table 4.2, where blood flow has the units of $\frac{ml}{g \text{ min}}$ and the rate constants have units of $\frac{l}{min}$. As listed in table 4.2, the calculated

value of rate constants and blood flow as indicated by the filled diamond are in good agreement with their initial values (filled spade) used in generating the time activity curve. It should be mentioned that in table 4.2 the initial values of blood flow (F) and the rate constants (Ls), marked by the filled spade were obtained using the value of the fixed parameters given in table 4.1. Theoretically the initial and calculated values of flow and the rate constants should be the same. However, in practice this is not achievable because of the iterative process of least squares fitting. Using initial parameter estimates the program calculates the sum of the squares of the differences between the "experimental curve" points and those of a curve predicted from the initial parameter estimates. The initial parameters are then incremented a number of times and the sum of squares of the differences recalculated for each increment. From parabolic fit of the sum of squares to each parameter, each parameter is adjusted to minimize the sum of squares prior to the next iteration. A convergence parameter built into the program terminates the iterative process once all parameters vary by less than a small amount. That is, each parameter is close to the bottom of the parabolic least squares well, at a "global minima". Table 4.2 shows the calculated values of rate constants and the blood flow in our model, reported experimental values of Lassen [1988], Matsuda [1988], and Murase [1992].

Extraction efficiency	Tissue density	Permeability surface area	Fraction of agent trapped
	g/ml	ml/g/min	†
0.80	1.03	1.25	0.60

Table 4.1. Values of the fixed parameters in the four compartmental model [Andersen, 1986; Lee, 1988].

Flow	L(1,2)	L(2,1)	L(3,2)	L(4,1)
ml/g/min	l/min	ml/g/min	l/min	l/min
0.800♣	0.658♣	0.640♣	0.973♣	0.948♣
0.7 ± 0.08*	0.7 ± 0.11*	0.5 ± 0.11*	0.8 ± 0.12*	0.0*
0.4 ± 0.03※	0.4 ± 0.04※	0.4 ± 0.03※	0.9 ± 0.05※	1.1 ± 0.1※
0.37 ± 0.1♣	0.6 ± 0.18♣	0.3 ± 0.08♣	0.6 ± 0.12♣	0.09 ± 0.0♣
0.787♦	0.650♦	0.630♦	0.970♦	0.950♦

Table 4.2. Values of the dependent parameters in the compartmental model.

- ♣ Data used for generating time-activity curve.
- * Data measured experimentally by Lassen [1988].
- ※ Data measured experimentally for gray matter by Matsuda [1988].
- ♣ Data measured experimentally by Murase [1992].
- ♦ Data calculated in our model when no error was introduced.

According to Lassen's study [1988], the conversion rate of lipophilic to hydrophilic forms, $L(3, 2)$, in the brain averaged $0.8 \pm 0.12 \text{min}^{-1}$. Matsuda [1988] has also reported the average value of $0.92 \pm 0.1 \text{min}^{-1}$ for the conversion rate whereas, Murase [1992] has reported the value of $0.69 \pm 0.09 \text{min}^{-1}$. The conversion rate calculated in this study has a value of 0.97min^{-1} . Similarly, the reported value of the blood flow is $0.7 \pm 0.08 \frac{\text{ml}}{\text{g min}}$, [Lassen, 1988], $0.4 \pm 0.03 \frac{\text{ml}}{\text{g min}}$, [Matsuda, 1988], and $0.53 \pm 0.05 \frac{\text{ml}}{\text{g min}}$, [Murase, 1992]. The calculated value for blood flow in this study was $0.787 \frac{\text{ml}}{\text{g min}}$. The agreement between the initial rate constant values and those retrieved from fitting to the generated total activity curve is close, verifying that the computer code was operating correctly.

The time-activity curves for the four compartments were obtained from the initial parameter values. These curves are shown in Figs. 4.1 through 4.4 respectively. As shown in the figures, for compartments one, two and four there was a rapid increase followed by a rapid decrease in the amount of activity over the first two minutes and after five minutes the activity was almost equal to zero. However, in compartment three, there was a gradual increase in the activity and the maximum activity was reached five minutes after administration of $Tc-99m-HMPAO$ and it stayed at this level for the time remaining in the experiment. Since the half life of $Tc-99m$ is 6 hours and the duration of the experiment was only 10 minutes, it was therefore assumed that the duration of the experiment was shorter than any significant radioactivity decay. As a result, the input functions were not modified to incorporate the decay process. Although compartments three and four are both irreversible trapping compartments (Figs. 4.3 and 4.4), their shapes are not similar. The reason is that in compartment three the tracer activity reaches a maximum and remains constant thereafter. Since it is defined as a hydrophilic tissue compartment, there is no outflow from it, and once the tracer traps in the tissue it remains there. On the other hand, compartment four is a hy-

drophilic blood compartment and due to the blood circulation throughout the body it has an out flow path, $L(4, 0)$. Consequently, in compartment four the tracer activity approaches zero as the time progresses.

As mentioned earlier, in clinical situations it is not possible to obtain the amount of activity in each compartment separately. The image is the sum of the activity in all four compartments at a specific point on their respective time activity curves. This is equivalent to obtaining the time-activity curve for compartment five in Fig. 3.3. A plot of activity vs time for compartment five is shown in Fig. 4.5. Here the maximum activity occurs at about 1.5 to 2.0 minutes after administration of $Tc-99m-HMPAO$, and five minutes after this administration, the activity reaches a steady state or equilibrium level.

It was discussed in the previous chapter that blood flow and extraction efficiency are related through the following relationship (eqn. 3.18):

$$E = 1 - e^{\left(\frac{-PS}{F}\right)}$$

A graph of extraction efficiency vs blood flow is shown in Fig. 4.6, from which it is apparent that there is a negative relation between the two parameters, i.e. as the flow increases the extraction efficiency decreases. Looking at the graph it will be clear that a variation of 40% in the flow will yield a difference of about 20% in the value of the extraction efficiency (E). However, in the present study, E has been taken to be a constant and the value assigned to it was that most used in the literature ($E = 0.8$) [Lee, 1988].

Fig 4.7 shows a plot of total activity of the blood and the brain tissue (compartment 5) versus time. The generation of each time activity curve was based on a constant blood flow value and calculation of rate constants using equations 3.25, 3.27, 3.28, and 3.29 given in chapter 3. The outer graph (open circle) with the maximum activity level has a flow value of $0.5 \frac{ml}{g \text{ min}}$, while the middle plot (closed circle)

represents a graph with a flow value of 0.7. Finally, a blood flow of 0.9 gives the lowest activity level (open triangle). The point to note is that the difference in the activity level between the graphs in this figure is maximum in the first two minutes, where the activity reaches its peak, and for the steady state level this difference is very small. That is, in the first two minutes, the total time activity curve of $Tc-99m-HMPAO$ is affected by the blood flow while it becomes almost independent of the flow value thereafter. Therefore, in order to obtain the most information about blood flow it is best to acquire the data before $Tc-99m-HMPAO$ reaches its steady state.

A similar study was also conducted to determine the effect of varying the rate constants on the total time activity curve. Flow and extraction efficiency were assumed to have constant values, and each rate constant was varied up to $\pm 75\%$ of its initial value, while keeping the other rate constants at their initial values. It was found that the clearance of lipophilic material from blood to tissue, $L(2, 1)$ had the maximum effect on the total time activity curve, while the other three rate constants had less effect. Fig 4.8a shows a plot of activity versus time when $L(2, 1)$ was varied from -75% to $+75\%$ of its original value of 0.632. As $L(2, 1)$ increases, the amount of activity also increases. Tables 4.3a, 4.3b, 4.3c, 4.3d show the values of the activity at its maximum and equilibrium levels when all the rate constants are varied from -75% to $+75\%$ of their initial values one at a time. The change in activity was higher when steady state level was reached for all the rate constants. The effect of varying each rate constant on the equilibrium level of the total time activity curve is plotted in Fig. 4.8b. As indicated above, changing $L(2,1)$, which governs the clearance of lipophilic material from blood to tissue, had the greatest effect on the equilibrium level of the total time-activity curve. The least change was for $L(4,1)$, the rate of trapping in blood, as a variation of $\pm 75\%$ in $L(4,1)$ only led to a change of $\pm 3\%$ in the equilibrium level of the total time-activity curve.

In the study of the system with added noise, one can define upper and lower bounds to indicate the range of allowable variation for each rate constant. This is useful because as described in the *SAAM* manual, it constrains their values to physically acceptable ranges which often leads to a reduction in the number of iterations required for convergence. The above experiment, in conjunction with clinical data, could be used in a clinical case to define upper and lower rate constant limits for that clinical study. In the present study of the system with added noise, a wider range was chosen to accommodate all possible variations in clinical situations. By doing this, however, one might possibly encounter local minima in the sum of squares parabolic fit. In simulation studies, this problem can be overcome by selecting the starting point close to the true minimum value. However, in clinical situations this is not feasible since the actual or true value is not known. The solution there is to repeat the experiment with several starting points to check the convergence. A global minimum is obtained if the fits converge to the same or similar parameter values.

% Var.	Max. point	Equil. Level	% Var.	Max. point	Equil. Level
+ 10%	0.085	0.0230	- 10%	0.086	0.025
+ 20%	0.085	0.0226	- 20%	0.086	0.026
+ 40%	0.085	0.0210	- 30%	0.086	0.029
+ 75%	0.084	0.190	- 75%	0.088	0.035

Table 4.3a : Value of activity at its maximum and equilibrium level when $L(1, 2) = 0.650$ is varied from -75% to $+75\%$, keeping $L(2, 1)$, $L(3, 2)$, and $L(4, 1)$ at their initial values.

% Var.	Max. point	Equil. Level	% Var.	Max. point	Equil. Level
+ 10%	0.087	0.027	- 10%	0.084	0.022
+ 20%	0.088	0.029	- 20%	0.083	0.019
+ 40%	0.092	0.034	- 30%	0.080	0.015
+ 75%	0.099	0.042	- 75%	0.076	0.0062

Table 4.3b : Value of activity at its maximum and equilibrium level when $L(2, 1) = 0.630$ is varied from -75% to $+75\%$, keeping $L(1, 2)$, $L(3, 2)$, and $L(4, 1)$ at their initial values.

% Var.	Max. point	Equil. Level	% Var.	Max. point	Equil. Level
+ 10%	0.0856	0.025	- 10%	0.0855	0.023
+ 20%	0.0857	0.026	- 20%	0.0855	0.022
+ 40%	0.0857	0.027	- 30%	0.0854	0.019
+ 75%	0.0857	0.028	- 75%	0.0852	0.011

Table 4.3c : Value of activity at its maximum and equilibrium level when $L(3, 2) = 0.970$ is varied from -75% to $+75\%$, keeping $L(1, 2)$, $L(2, 1)$, and $L(4, 1)$ at their initial values.

% Var.	Max. point	Equil. Level	% Var.	Max. point	Equil. Level
+ 10%	0.0855	0.024	- 10%	0.0856	0.0244
+ 20%	0.0855	0.024	- 20%	0.0857	0.0246
+ 40%	0.0854	0.0239	- 30%	0.0858	0.0248
+ 75%	0.0852	0.0235	- 75%	0.0860	0.0252

Table 4.3d : Value of activity at its maximum and equilibrium level when $L(4, 1) = 0.950$ is varied from -75% to $+75\%$, keeping $L(1, 2)$, $L(2, 1)$, and $L(3, 2)$ at their initial values.

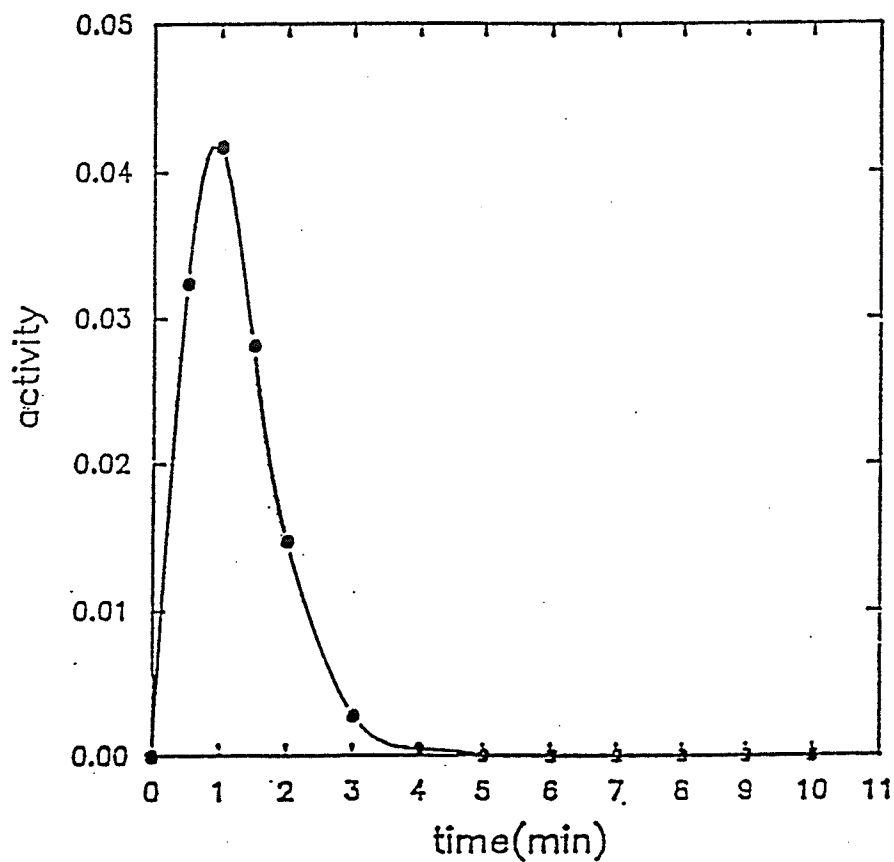


Fig. 4.1 : Plot of activity in compartment one over a period of 10 minutes, where compartment one is the lipophilic, diffusible tracer in the blood.

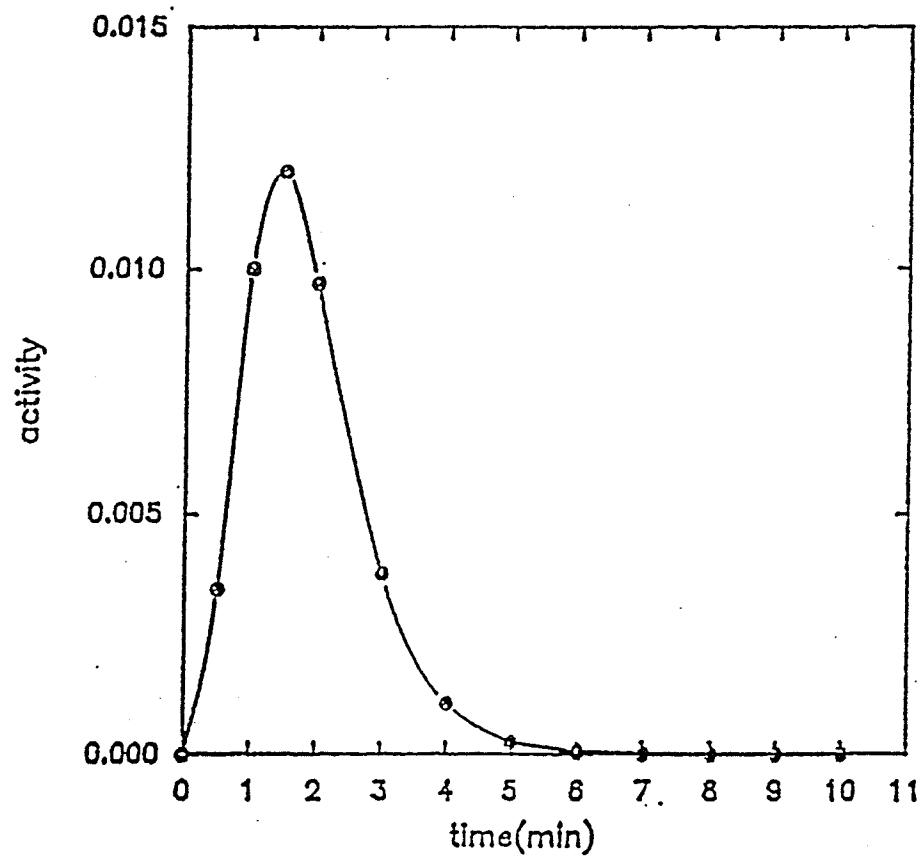


Fig. 4.2 : Plot of activity in compartment two over a period of 10 minutes, where compartment two is the lipophilic, diffusible tracer in the brain tissue.

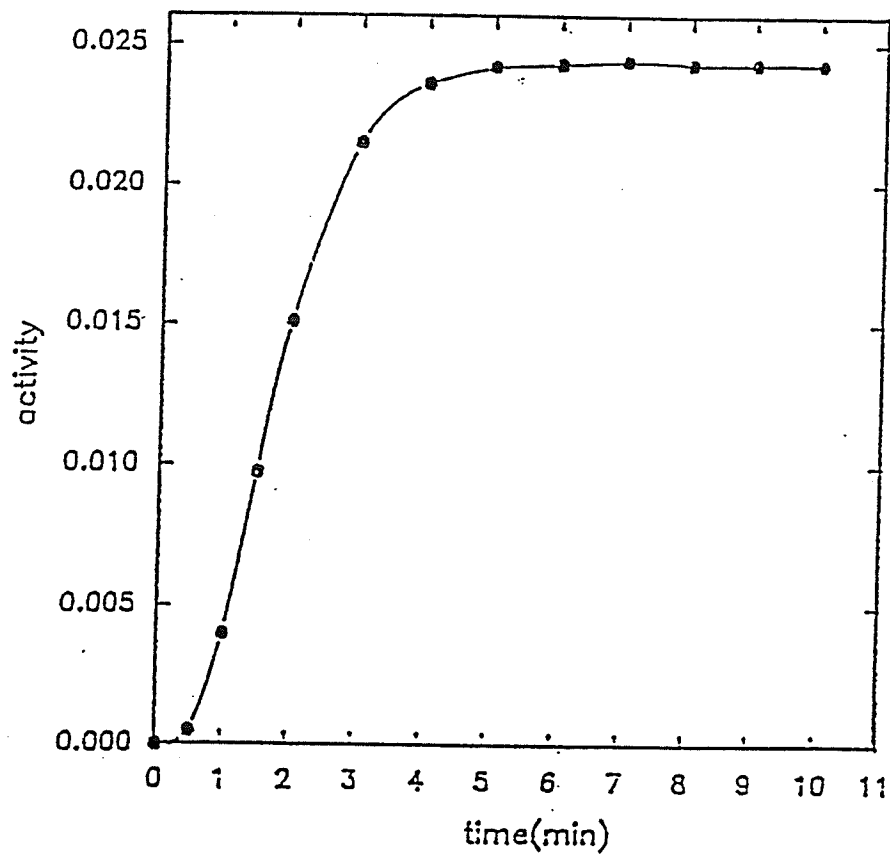


Fig. 4.3 : Plot of activity in compartment three over a period of 10 minutes, where compartment three is the hydrophilic, nondiffusible tracer trapped in the brain tissue.

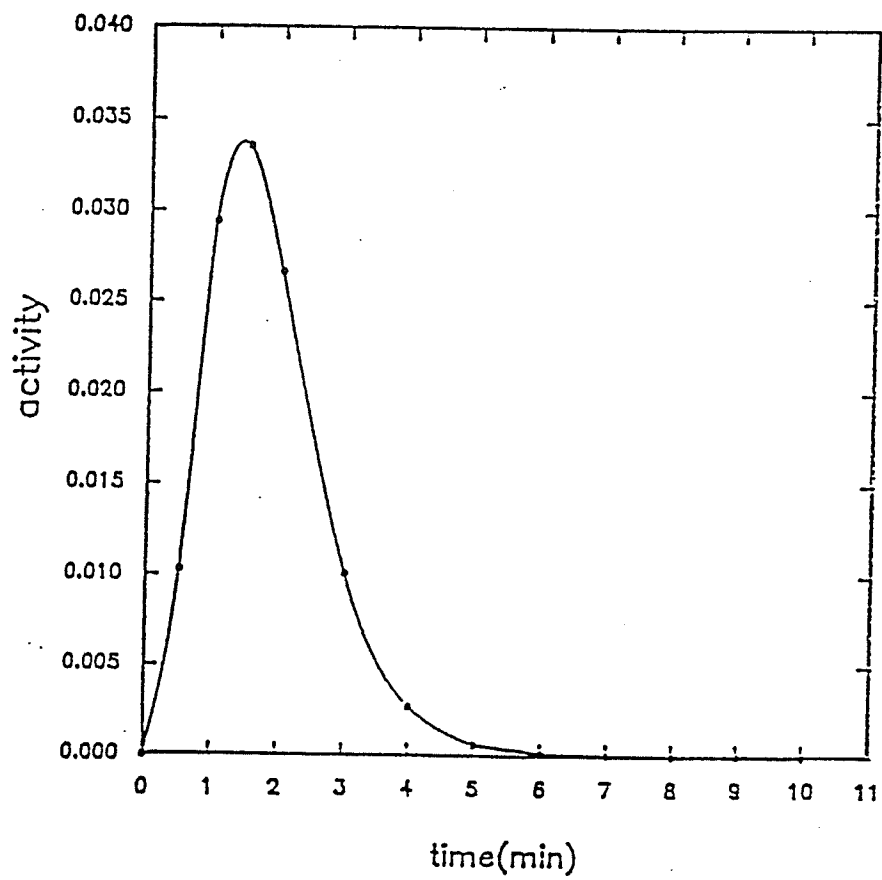


Fig. 4.4 : Plot of activity in compartment four over a period of 10 minutes, where compartment four is the hydrophilic, nondiffusible tracer trapped in the blood.

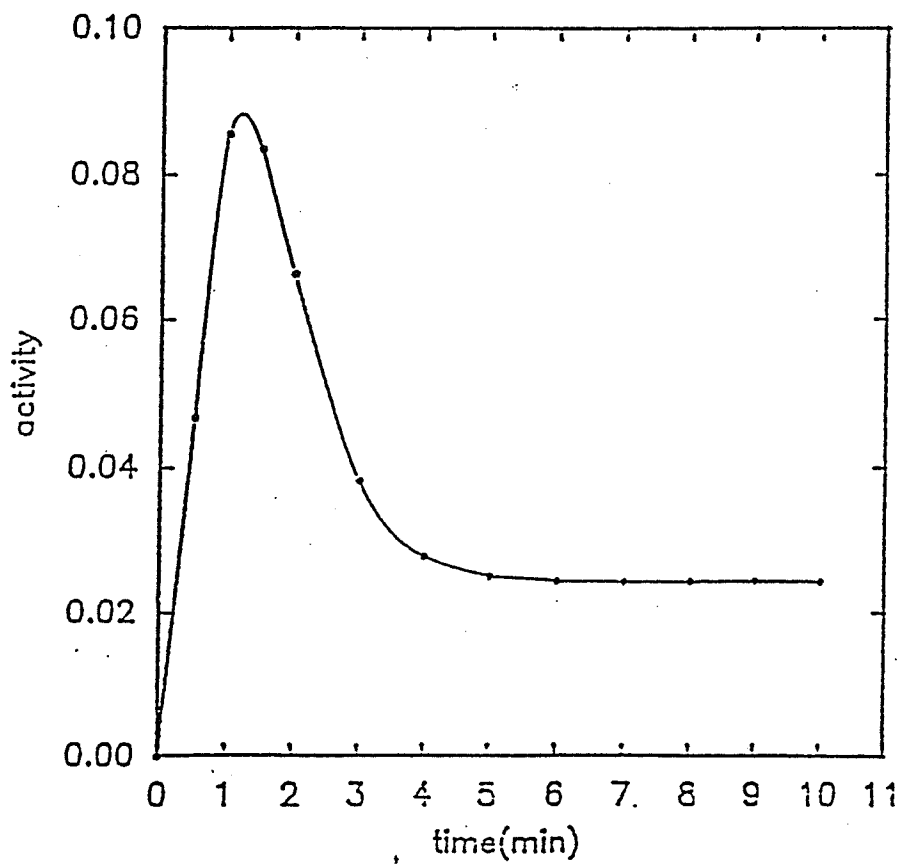


Fig. 4.5 : Plot of total activity of the four compartments, compartment 5, over a period of 10 minutes.

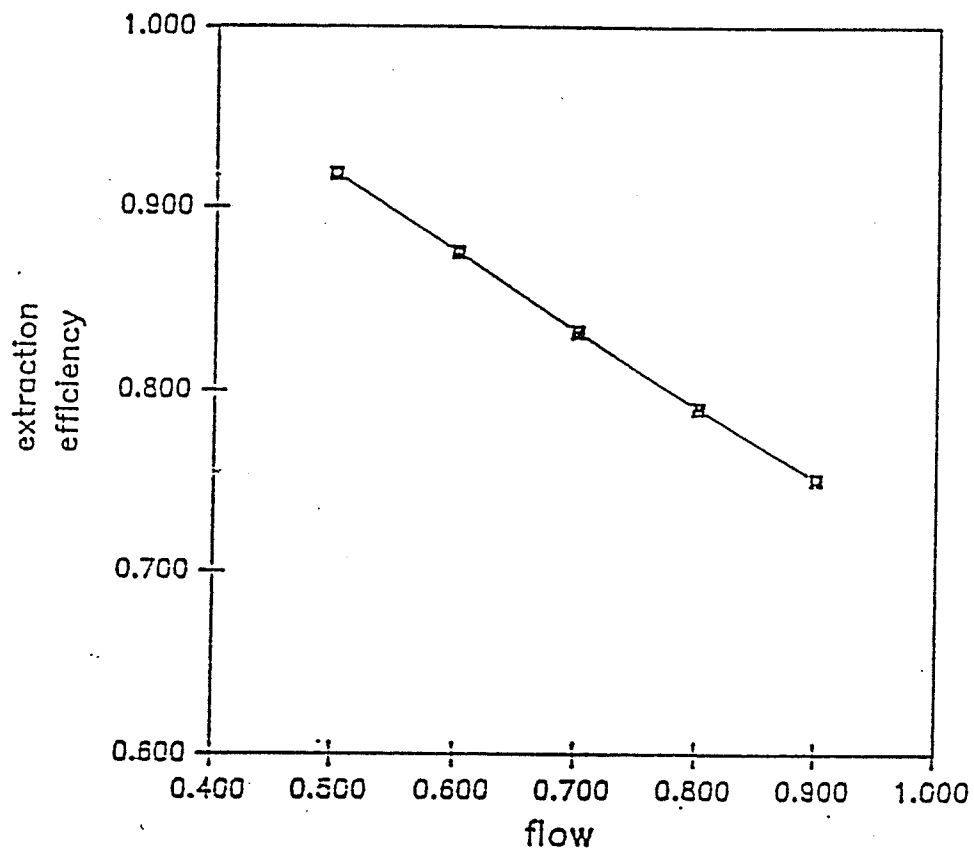


Fig. 4.6 : Relation between extraction efficiency and blood flow. A variation of 40% in flow produced a difference of 20% in value of extraction efficiency.

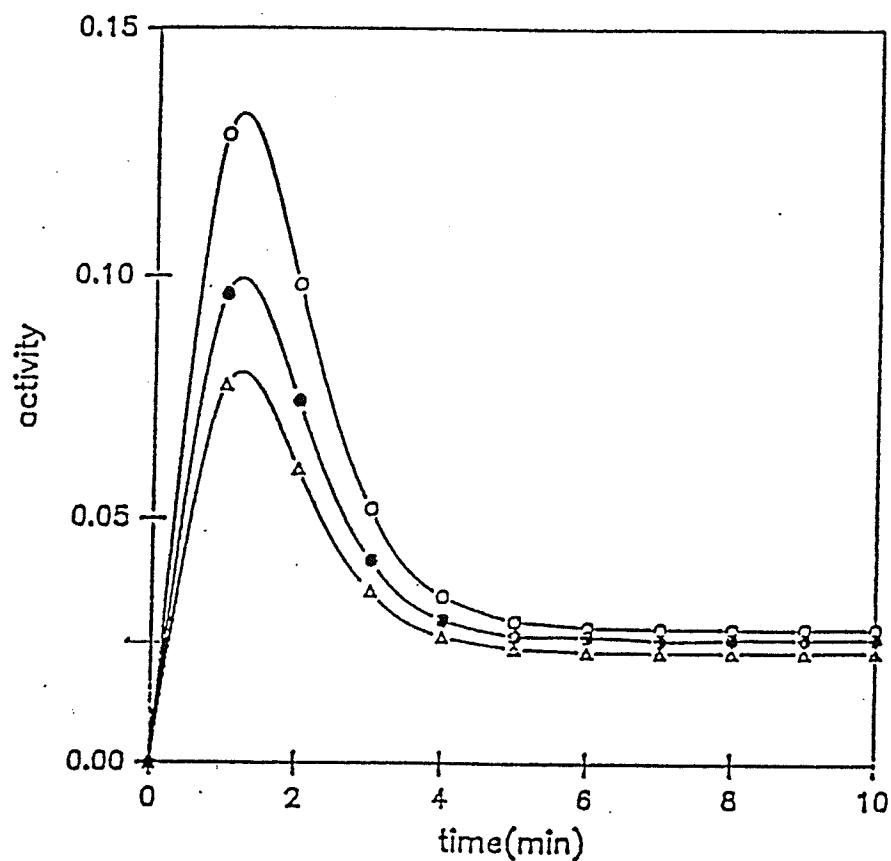


Fig. 4.7 : Graph of total activity vs time for different flows. The outer graph (open circle) has a flow value of 0.5ml/g/min, the middle plot (closed circle) has a flow value of 0.7ml/g/min, and the open triangle represents the flow of 0.9ml/g/min.

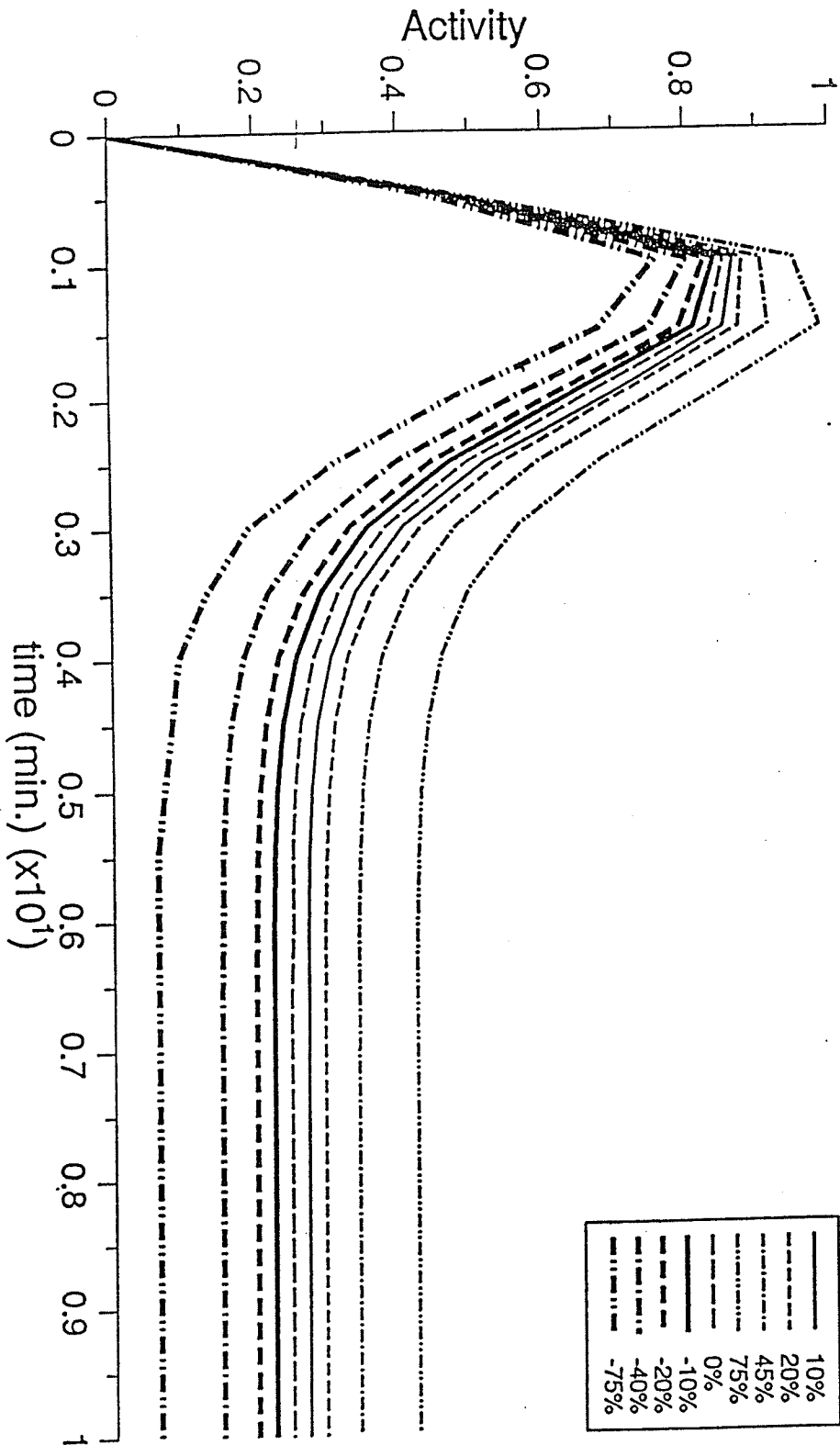


Fig. 4.8a : Plot of total time activity curve when $L(2, 1)$ is varied from -75% to $+75\%$ of initial value.

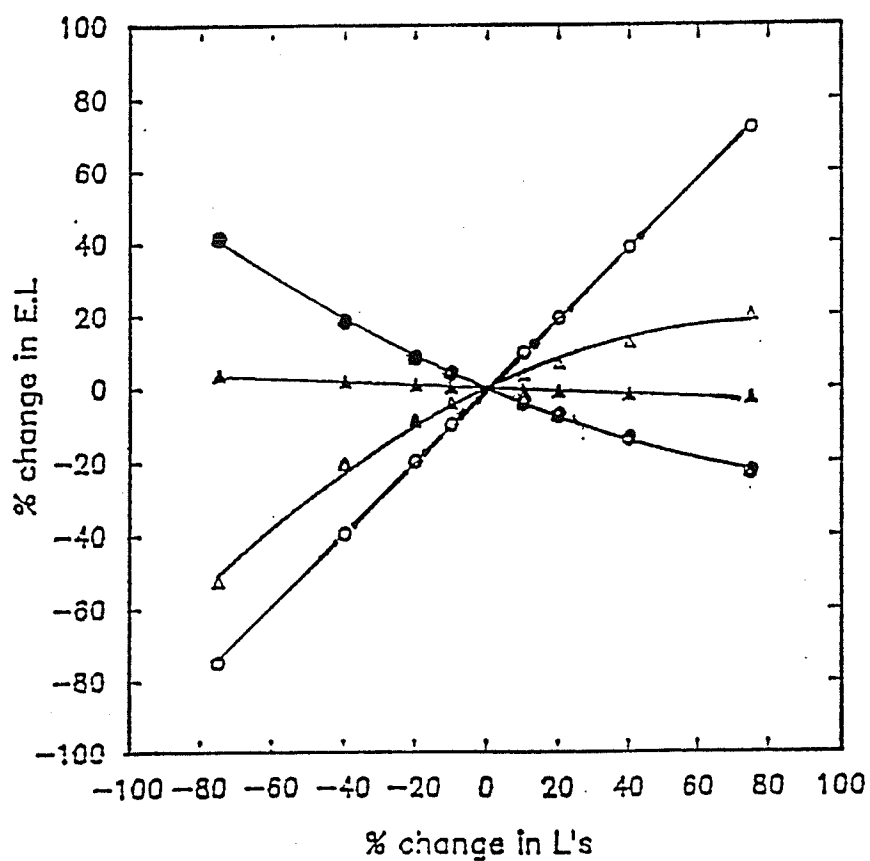


Fig. 4.8b : Graph of equil. level of activity vs rate constant as each of the rate constant are varied by $\pm 75\%$.
 Open circle represents the change in $L(2, 1)$, filled circle represents $L(1, 2)$, open triangle represents $L(3, 2)$, and filled triangle represents $L(4, 1)$.

4.4. Calculation of the Rate Constants and Flow with Added Error

In order to study the effect of noise on the precision of the rate constants and blood flow, Gaussian noise [Papoulis, 1965] was introduced to the total time activity curve repeatedly. That is, to determine the likely error involved in measurements of regional cerebral blood flow, the calculated total time activity curve was modified by the addition of various amounts of random Gaussian noise. To do this, ten points were selected along the total time activity curve over an interval of 10 minutes. Each point was spaced equally one minute apart on the total time activity curve. It should be noted that a minimum of four sample points are required to find the value of the four rate constants. However, it is assumed that selection of four points make the finding of the rate constants and flow less accurate.

The arterial curve is assumed to have a functional form rather than being described by a series of experimental points. Such an assumption is valid since the experimental errors involved in obtaining the arterial curve are much smaller than the errors associated with the total time activity curve. This arises since the counting period of the arterial samples can be adjusted to provide a very small error on each point. The functional form for the arterial curve can be determined by fitting some function to the experimental points. This fit is also independent of the simulation. Thus, the parameters of the fit for the arterial curve can be determined. In our work, the arterial curve was taken from the literature [Lee, 1988].

Next, the total time activity curve with added noise, as specified by the user-assigned standard error was generated. In doing so, a software program was developed to generate noisy brain curves. The program used the International Mathematical and Statistical Library (*IMSL*) routines to generate Pseudo-random number deviates, R , by transforming uniform deviates to normal deviates using the inverse normal routine. The analysis was based on the generation of random numbers using the linear congruential method [Lehman 1951]. In this method, a sequence of integers I_1, I_2, I_3, \dots each

between 0 and $m - 1$ were generated by the following recurrence relation,

$$I_{j+1} = a I_j + c \quad (4.1)$$

where m is a large number and called the modulus, a and c are positive integers called the multiplier and the increment respectively. The sequence starts from a given seed number I_0 , and returns the real number $\frac{I_{j+1}}{m}$ which is strictly between 0 and 1.

Next, a transformation was used to transfer the generated uniform deviate into the normal deviate. The desired transformation was given by

$$P = \frac{1}{\sqrt{2\pi}} \int_{-\infty}^R e^{-\frac{t^2}{2}} dt \quad (4.2)$$

for a given value of P , where P is the input value in the range (0, 1), R is the output value of the inverse normal (0, 1) probability distribution function. The computation was then reduced to the evaluation of the inverse error function in the interval (0, 1), where the error function and complemented error function were defined by,

$$erf(R) = \frac{2}{\sqrt{\pi}} \int_0^R e^{-t^2} dt \quad (4.3)$$

$$erfc(R) = \frac{2}{\sqrt{\pi}} \int_R^{\infty} e^{-t^2} dt \quad (4.4)$$

Random normal deviates which define the noisy points on the total time activity curve were obtained by transforming the output according to

$$Y_i = R_i SE + \mu_i \quad (4.5)$$

for i in (1, 2,, NR). In equation 4.5, μ_i is the actual noiseless point and SE is assigned standard error, R_i is the output vector of length NR containing the normal (0, 1) random numbers, and NR is the input number of deviates to be generated.

4.4.1. Computer Simulations with the Presence of Noise

A study was conducted to relate the mathematical terminology of noise, SE , to a more clinically relevant concept, namely the mean percentage error associated with the points of the total time activity curve. More specifically, the mean percentage error is defined as the mean percent difference between the noisy and noiseless total time activity curves. To do this, for each standard error, SE , the percentage difference between each of the 10 points on the noisy total time activity curve and the corresponding points on the noiseless curve was determined. The average percentage difference was taken for each standard error and the results are presented in table 4.4.

Standard Error (SE)	% Difference
0.005	$\pm 2\%$
0.01	$\pm 4.3\%$
0.05	$\pm 9.5\%$
0.1	$\pm 26.5\%$
0.5	$\pm 78\%$

Table 4.4 : % variation on the time activity curve for different standard errors.

As the standard error increased the percent variation also increased. For the lower noise level the percentage variation of points on the total time activity curve was small and is not likely to be clinically achievable. On the other hand, for the largest standard error the variation was likely too large to be useful in clinical studies. In practice a variation of about $\pm 15\%$, which correspond to standard errors in the range of 0.05 to 0.1, is the range that can be useful clinically [Nickel, 1989].

The procedure for generating noisy total time activity curves was performed six hundred times for the selected ten points and the assigned value of standard error. The procedure of using these same points to generate noisy total time-activity curves was carried out for five different standard errors. As a result of this, three thousand noisy total time activity curves were generated and used as input curves for the computer simulation. Therefore, for each standard error assigned, rate constants and the blood flow were calculated six hundred times. Assuming the blood flow and the rate constants have normal distribution, their mean and standard deviation were then calculated.

It should be mentioned that an upper bound of 5.0 and lower bound of 0.0001 were assigned to each rate constant during the computer simulation [Berman, 1974]. Although selecting such a wide range, for each rate constant may include the presence of local minima, it will accommodate the range for all clinical situations as discussed earlier.

Figs. 4.9 and 4.10 represent the values of the mean and their standard deviation using 600 simulations for the rate constant, $L(2,1)$, and blood flow, F , respectively. Figs. 4.11 to 4.15 illustrate the distribution of blood flow estimates during 600 simulations. Also shown in the Figs. is a spike indicating the starting value of the iteration. These histograms (Figs. 4.11 to 4.15) show the relative probability of obtaining a particular value of blood flow when fitting data that had associated standard errors of 0.005, 0.01, 0.05, 0.1, and 0.5 respectively. It was observed that at the lower noise level (standard error of 0.005), the centre of the distribution was closer to the input value of $0.787 \frac{ml}{g \text{ min}}$ than at higher SE values as one would expect because of the asymmetry of the peaks. However, it was observed that the blood flow distribution generated in this experiment for a given standard error was not Gaussian. For a higher noise level (standard error of 0.5) the spread in the distributions was much larger, and also the distribution was less normal.

Since the blood flow distribution as shown in Figs. 4.11 to 4.15 were not Gaussian, the use of standard deviation to describe the spread of blood flow estimate generated in this study was not appropriate. Instead, the results of the simulations performed were expressed in terms of a given percentile, the values of blood flow below and above which percentile of the simulated results falls [Bews, 1990]. Such an approach not only indicates the major impact of noise on the accuracy of blood flow estimates, but also the relatively high probability of estimating blood flow values which are well removed from the true (or input) flow value. Fig. 4.16 illustrates an estimate of the errors incurred in predicting the flow as a function of the standard error associated with the experiment. The effects are seen to be large, with 54% of the experiment values lying between the mean and 95% percentiles, and 22% between the mean and the 5% percentiles. At a standard error of 0.1, the above percentages increased to 65% and 25% respectively.

Table 4.5 presents the percent difference of the mean blood flow from its true value of 0.787 for various standard errors.

Standard Error (SE)	% Difference from true value
0.005	1.7
0.01	3.0
0.05	5.5
0.1	9.3
0.5	32

Table 4.5 : % variation of mean blood flow for different standard errors.

As one can observe from the table, the % difference of mean flow from the true value (0.787) increases as the standard error increases. This could be due to the fact that flow distribution for various standard errors is not a normal distribution. Since a normal distribution is symmetric one would expect the mean to be the same regardless of the amount of error introduced. Another point to note is that the mean flow is always greater than the true value. This is likely due to the fact that the distribution of flow is skewed to the right hand side of the true value for all standard errors.

A study was also conducted to check whether the flow distribution for various standard error was independent of their initial value of $0.787 \frac{ml}{g \text{ min}}$. The selected boundary limits between which each parameter was allowed to vary was quite wide, resulting in the possibility of convergence to some local minima as mentioned earlier. To investigate this, the following test was performed.

For each blood flow frequency distribution points entirely outside the distribution, both above and below, were selected. From equation (3.25) which relates the blood flow to the rate constant $L(2, 1)$, a new initial estimate of $L(2, 1)$ was calculated from the above points. For each standard error, and each initial rate constant estimate corresponding to positions outside the blood flow frequency distribution, 10 simulations were performed and the blood flows re-determined. In all cases except for a standard error of 0.5, the newly calculated blood flows were within the original distributions. This strongly suggests that convergence was to a global minima rather than to some local minima.

The anomaly at 0.5 standard error can be explained as below. At large errors the individual noisy data points of the total time activity curve can assume negative values. Such values are not physically reasonable and are set to zero. For cases where several zero points were present, *SAAM* could not obtain a fit and under these conditions it returns to its input values.

The distribution for lower errors suggests the possibility of a double peak. This may be due to an insufficient number of simulations or to the existence of local minima. Although, the above test suggests that convergence was to the global minima, it has to be noted that the number of simulations for this test (20 simulations per standard error) was significantly less than the total number of simulations (600 per standard error). Therefore, the possibility still exists of local minima occurring in some of the simulations.

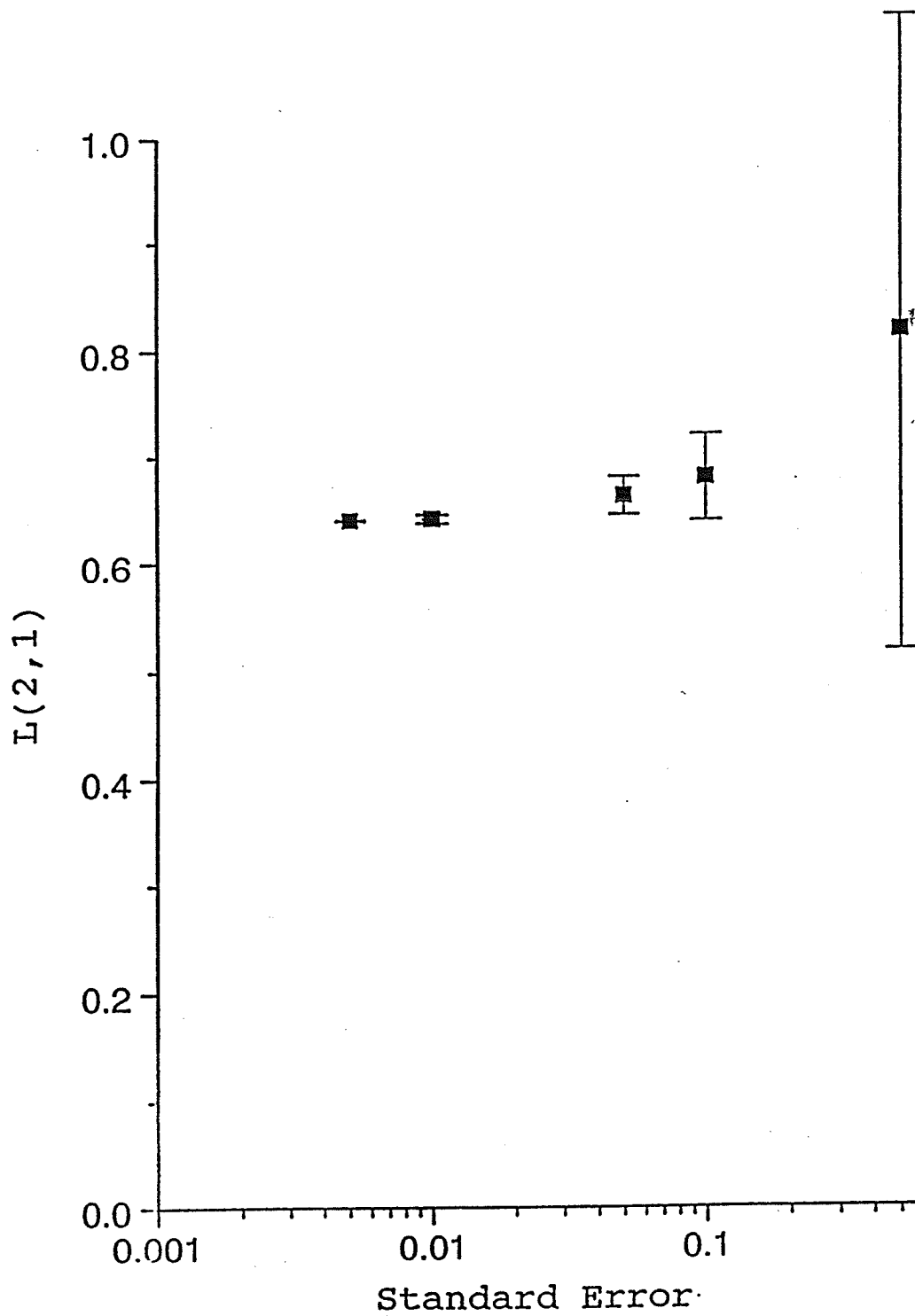


Fig. 4.9 : Graph of $L(2, 1)$ vs standard error.

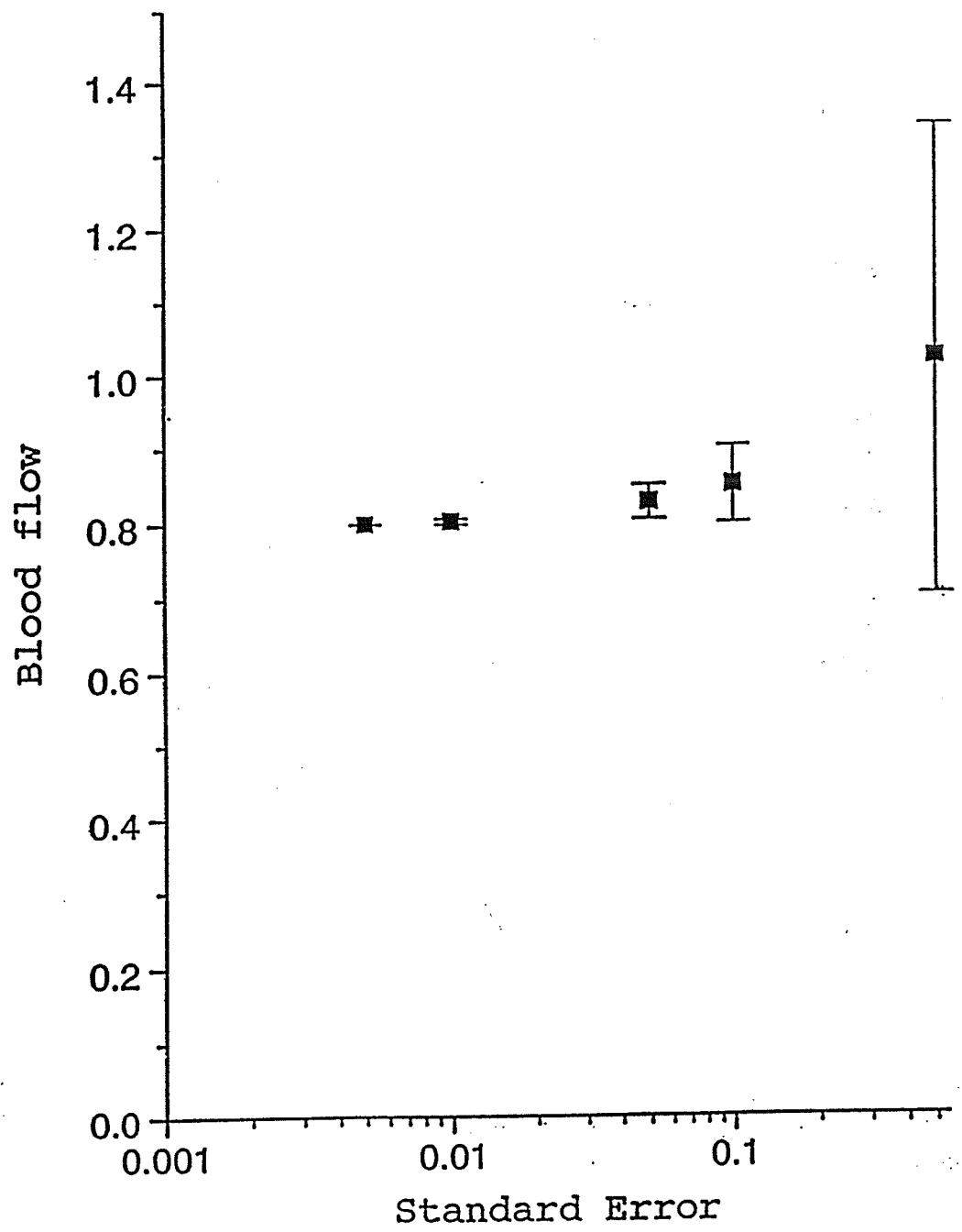


Fig. 4.10 : Graph of flow vs standard error.

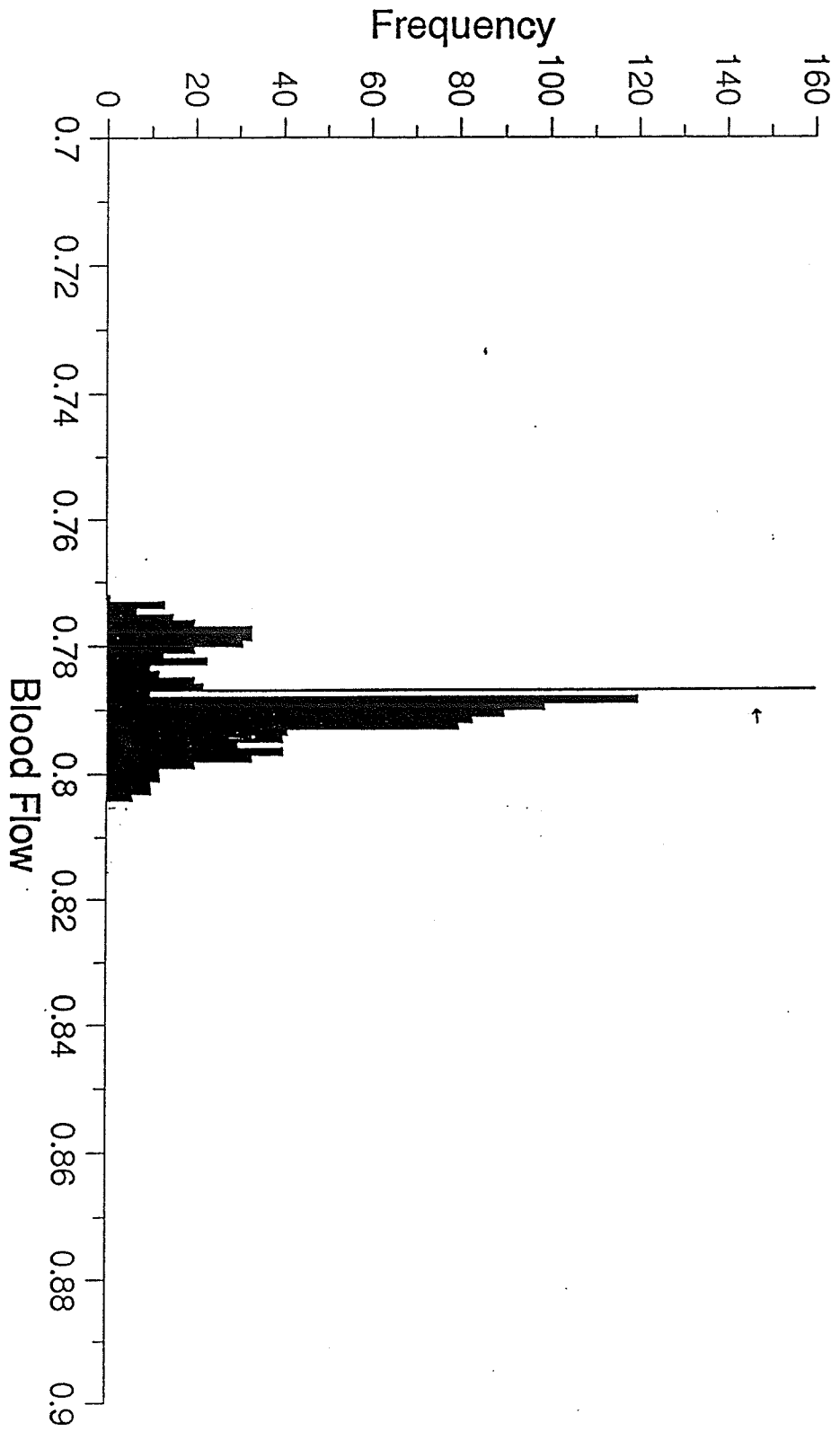


Fig 4.1.1 : Blood flow distribution for the standard error of 0.005.

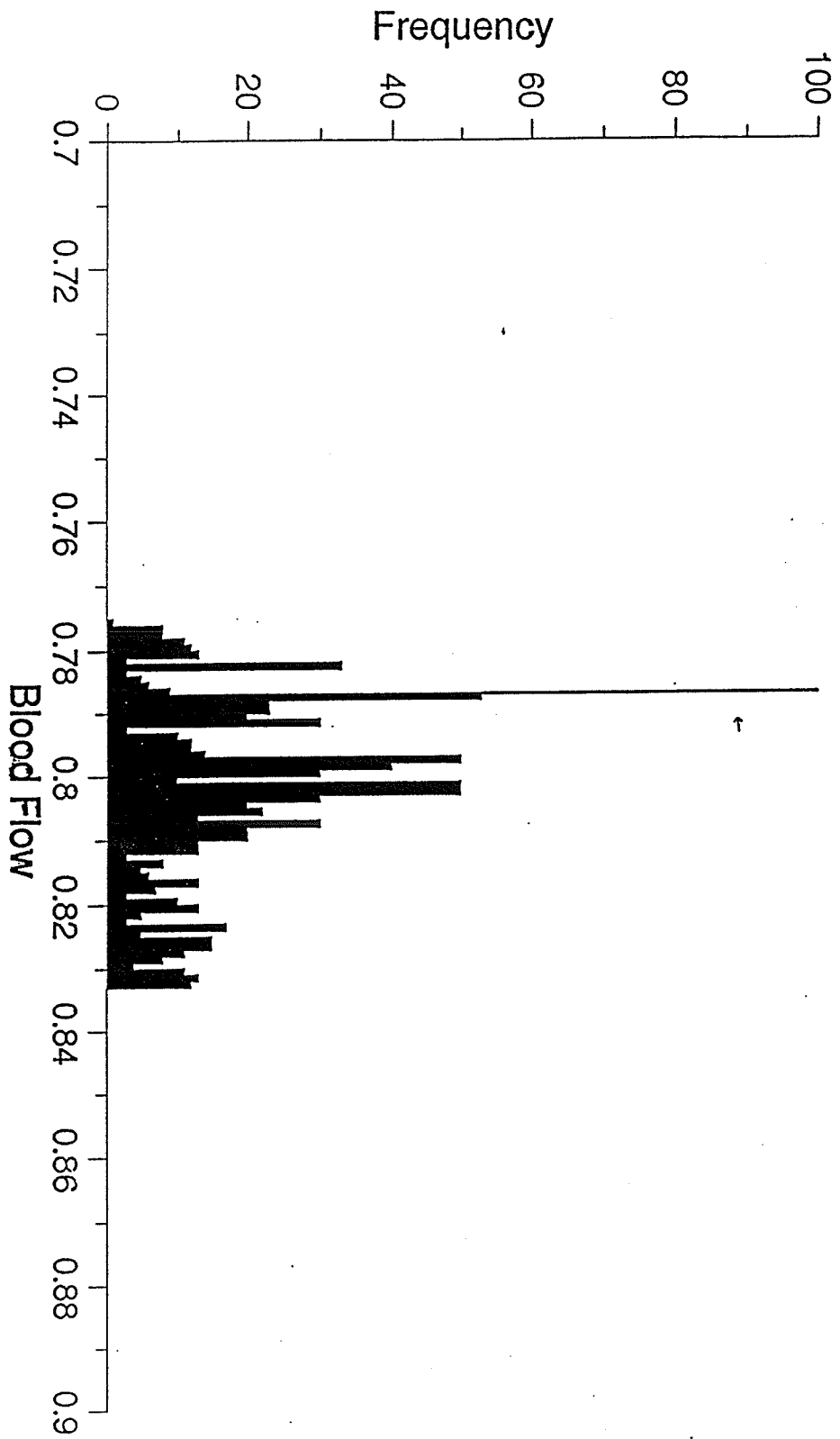


Fig 4.12 : Blood flow distribution for the standard error of 0.01.

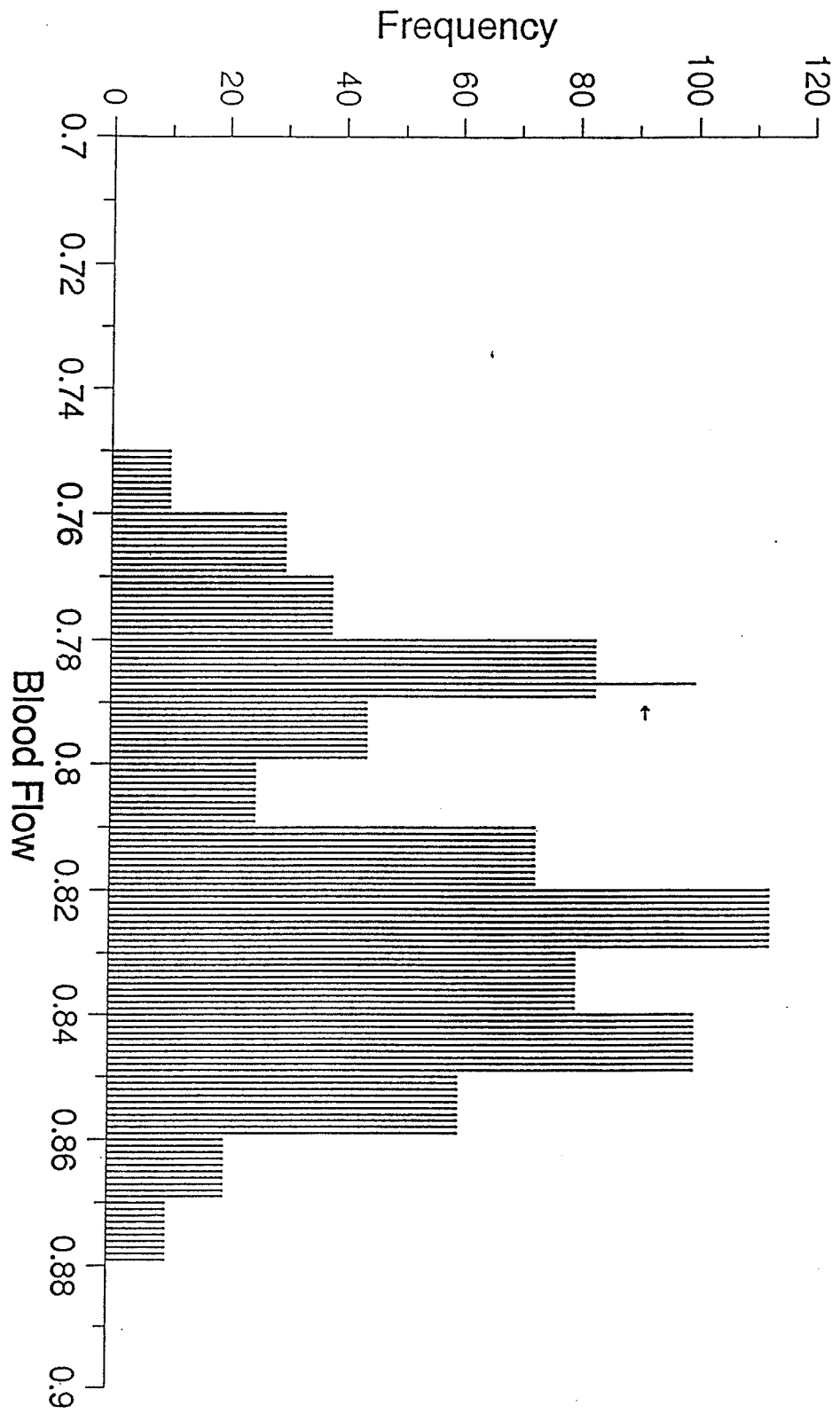


Fig 4.13 : Blood flow distribution for the standard error of 0.05.

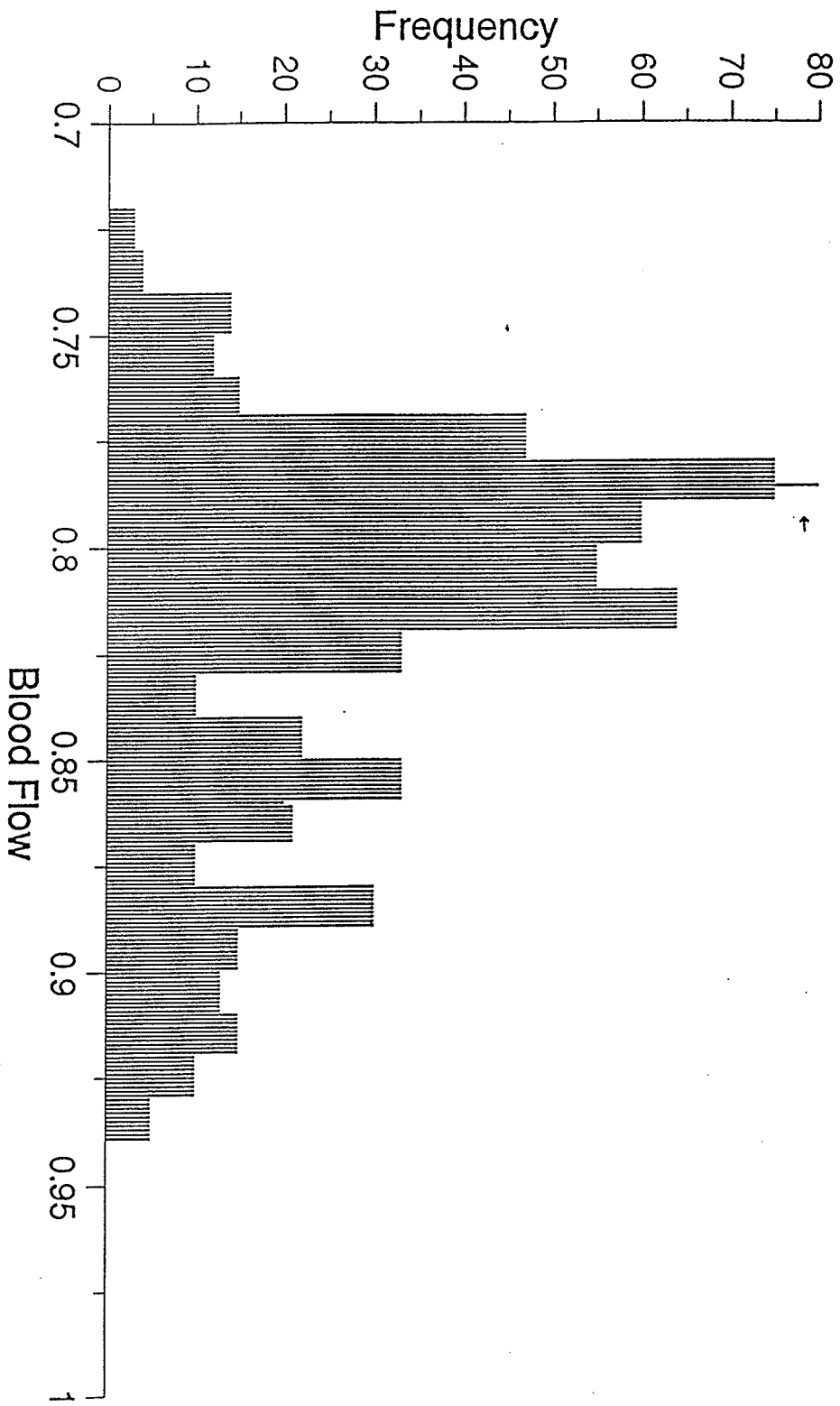


Fig 4.14 : Blood flow distribution for the standard error of 0.1.

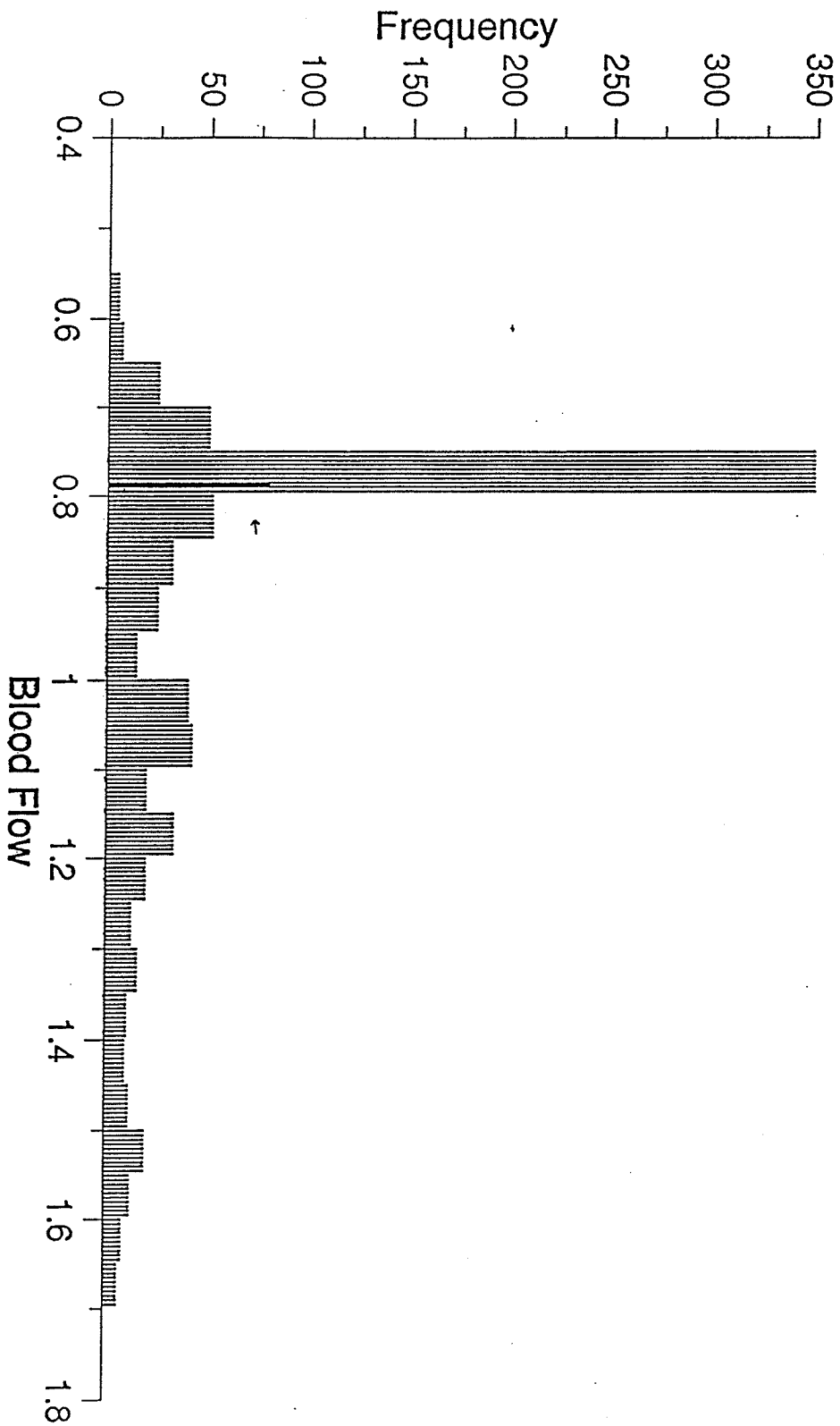


Fig 4.15 : Blood flow distribution for the standard error of 0.5.

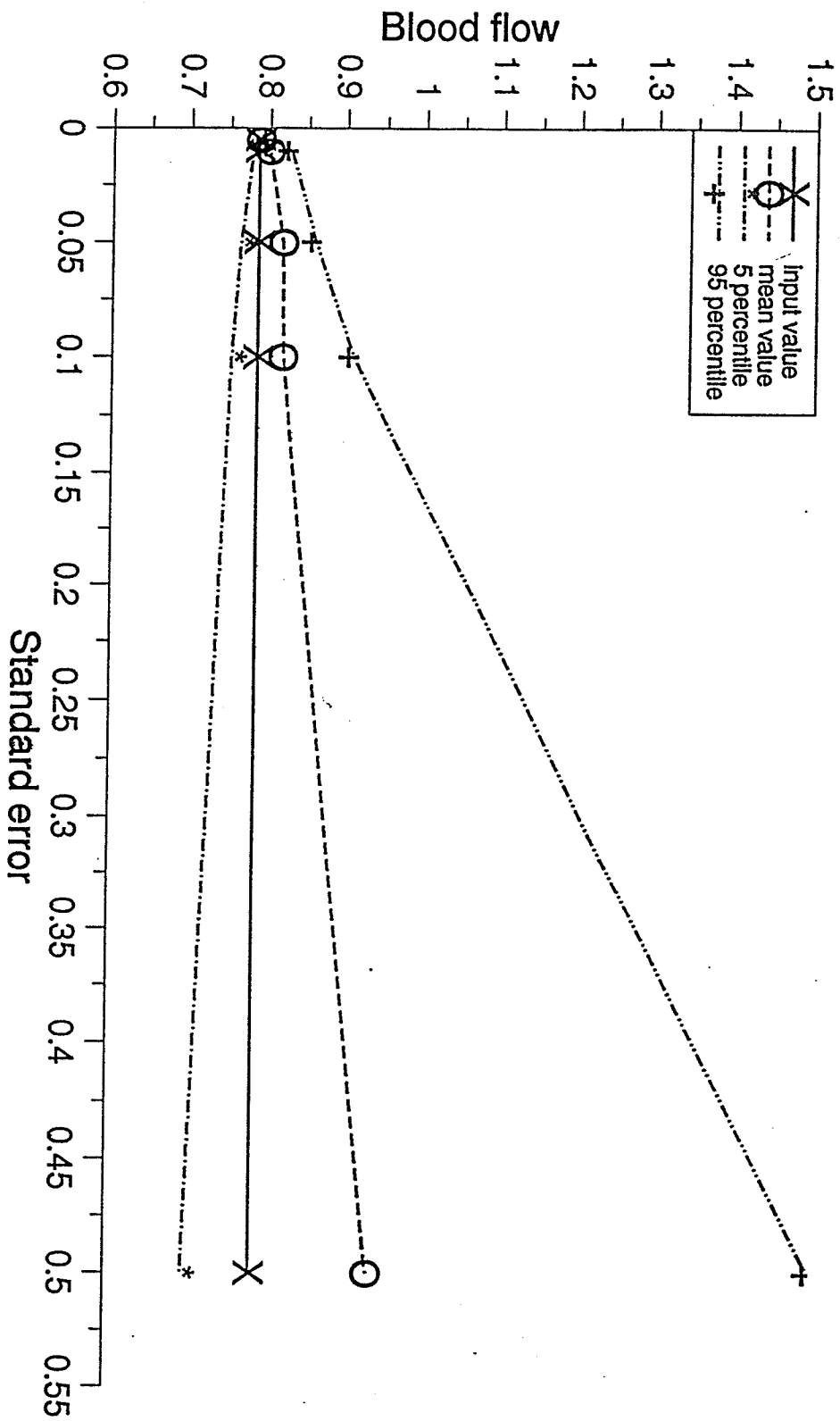


Fig 4.16 : Error incurred in the measurement of the blood flow.

Chapter 5

Discussion and Conclusions

It was the objective of this thesis to study compartmental modeling of the brain and investigate the determination regional cerebral blood flow with the radiopharmaceutical, $Tc-99m-HMPAO$, using a theoretical arterial blood curve. The proposed method was based on mathematical modeling of the brain and utilized computer simulation to study regional cerebral blood flow. This was done using a four compartmental model of the brain that describes the transport of $Tc-99m-HMPAO$ in the brain. The study assumed that $HMPAO$ passes through the blood-brain-barrier and localizes in brain tissue [Matsuda, 1988]. Also, from the practical point of view, it was assumed that the single pass extraction efficiency, E , for $HMPAO$ was constant throughout the brain and identical for all patients [Matsuda, 1988]. To carry out the simulation, a set of typical values for the rate constants in the compartmental model of $HMPAO$ and a typical arterial concentration curve were assumed. From these a theoretical total time activity curve was generated. The simulation experiment then consisted of carrying out a non-linear regression analysis to investigate the accuracy and precision of calculating the $rCBF$ when various amounts of Gaussian noise were added to the theoretical total time activity curve.

The experiment was divided in two parts. The first part was the simulation of $HMPAO$ kinetics with no error added to the total time activity curve. The typical rate constants of 0.651, 0.632, 0.978, and 0.948 [min^{-1}] for $L(1,2)$, $L(2,1)$, $L(3,2)$, and $L(4,1)$ were chosen in this study. The calculated value for the blood flow was found to be equal to $0.787 \frac{\text{ml}}{\text{g min}}$. The arrival of radioactivity in the brain occurred as a peak 1.5 to 2.0 minutes after intravenous injection of $Tc-99m-HMPAO$. This was followed by a

sharp decrease over the following 3.0 minutes. Then a steady state was reached for the remainder of the experiment.

Because of the complexity of the model, many variable parameters were involved. One of the aims in this work was to study the effect of individual variables on the total time activity curve. Consequently, computer tests were performed to check the effect of varying the rate constants on the time activity curve. Each rate constant was varied for a wide range of -75% to $+75\%$ of its original value, while keeping the other rate constants at their original value. The results obtained indicated that the rate constants involved in the trapping mechanism had the least effect on the activity curves and have minimal effect on the calculated blood flow. Future work should investigate the effect of fixing these parameters at appropriate values to reduce the complexity of the fit and hopefully to improve the precision of the blood flow measurement. On the other hand, $L(2, 1)$ which describes the clearance of lipophilic material from blood to tissue, had the greatest effect on the total time activity curve. The upper and lower bounds for each rate constant were selected wider than the range of variation expected in a clinical situation to ensure the presence of the global minima, and then entered as an input, to constrain the fitted parameters. Although selection of wider boundary limits will possibly increase the number of iterations to convergence, this was overcome by starting the simulation close to the true value. It was observed that in multi-parameter non-linear least squares curve fitting one must guard against convergence to local minima. This problem was alleviated in part by choice of the initial parameter estimate close to its known value. Also a technique for specifically checking for local minima by selecting initial parameter estimates corresponding to points outside the fitted parameter distribution was developed.

The second part of the experiment was to determine the likely error involved in the measurements of blood flow. The calculated total activity curve was modified by the addition of various amounts of random Gaussian noise. It was observed that the

blood flow distribution generated in the experiment for different standard errors was not Gaussian. Therefore, the use of a standard deviation to describe the precision or spread of the blood flow generated was not appropriate. Instead, results were expressed in terms of percentiles [Bews, 1990].

Since it was necessary to express the blood flow errors as percentiles, it is difficult to compare them with the errors on the input total activity curves. However, table 5.1 shows the correspondence between the mean percentage error of the points of the total activity curves and the percentile errors of the blood flow calculations. Thus, knowing the errors associated with a clinical study, one can predict the error in a blood flow determination.

As discussed in an earlier chapter, the work of [Good, 1987] demonstrated that offsets in the time origins of the total time activity and arterial curves were difficult to quantify and introduced additional errors to blood flow calculations. In the present work no time offsets were introduced, so that the blood flow errors presented above underestimate those that would likely be encountered in a clinical situation.

In this study a simulated theoretical total time activity curve was generated, and as mentioned earlier, it rose to a peak and dropped to a plateau over a time interval of six to ten minutes. Clearly, in order to sample this curve in a clinical *SPECT* environment, the individual scans must have a time duration of about one minute or less. This is not clinically feasible with most single detector *SPECT* scanners currently in use, but is possible with special purpose multiple detector systems. Fig. 4.7 shows that even over time intervals of less than one minute the activity changes appreciably. Thus, an experimentally measured total time activity curve will be a convolution of the "actual" time activity curve and the time aperture of the *SPECT* camera. To account for this convolution, modification of the flow compartmental model used in this work on theoretical noise analysis must be made before its application to clinical *SPECT*.

A more subtle point, not addressed in this work nor in the literature to date, is the fact that even in *SPECT* scans of less than one minute the activity distribution in the patient will change. This changing distribution will generate artifacts in the *SPECT* reconstructed images. Also, such short scans will contain relatively high noise from the poor counting statistics.

To extend the present work and possibly realize the aim of performing quantitative blood flow measurements using *SPECT*, several further studies should be performed. These include repeating the error analysis of the present study with the convolution technique to account for the *SPECT* imaging time: an investigation of the effects of reducing the number of fitted variables on the error of the blood flow measurements: and a dynamic phantom study to investigate artifact generation in *SPECT* images.

Standard error SE	Mean % error on input curve	Blood Flow		
		Mean	5 Percentile	95 percentile
0.005	$\pm 2\%$	0.788	0.777	0.799
0.01	$\pm 4.3\%$	0.80	0.780	0.828
0.05	$\pm 9.5\%$	0.818	0.765	0.860
0.1	$\pm 26.5\%$	0.819	0.754	0.910
0.5	$\pm 78\%$	-	-	-

Table 5.1 : Correspondence between the mean percentage error of the points of the total activity curves and the percentile errors of the blood flow calculations.

References

- Andersen A. R., Friberg H., Lassen N., et al., "Assessment of the arterial input curve for Tc-99m-d,l-HMPAO by rapid octanol extraction," *J. Cereb. Blood Flow Metab.* 8 (suppl 1), pp. S23-S30, 1988.
- Axelsson B., Msaki P. and Israelsson A., "Subtraction of Compton-Scattered Photons in single-photon emission computerized tomography," *J. Nucl. Med.* 25, pp. 490-494, 1984.
- Berman M., "SAAM Manual," U.S. Department of Health, Education, and Welfare, 1974.
- Berman M., and Shahn E., "Problems in the mechanization of isotope tracer data analysis," in *Proc. 1st IBM Med. Symp.*, IBM, New York, 1959.
- Bews J., Dunscombe P. B., Lee T. Y., et al., "The role of noise in the measurement of cerebral blood flow and partition using xenon-enhanced computed tomography," *Phys. Med. Biol.*, 35, no. 7, pp. 937-945, 1990.
- Bok B. D., Scheffel U., Goldfarb H. W., et al., "Comparison of Tc-99m complexes (NEP-DADT, ME-NEP-DADT and HMPAO) with IAMP-123 for brain SPECT imaging," *Nucl. Med. Comm.* 8, pp. 631-641, 1987.
- Biersack H. J., Grunwald F., Reichmann K., et al., "Functional brain imaging with single photon emission computed tomography using Tc-99m-labelled HMPAO," *Nucl. Med. Annual*, PP. 59-94, 1990.
- Budinger T. F. and Gullberg G. T., "Three dimensional reconstruction of isotope distributions," *Phys. Med. Biol.*, 19, pp. 387-389, 1974.

References

- Cheesman E. H., Blanchett M. A., Ganey M. V., et al., "Tc-99m-ECD: ester-derivatized diaminedithiol Tc complexes for imaging brain perfusion, [Abstract]," J. Nucl. Med. 29, pp. 788, 1988.
- Canning L., Nechvatal G., Cumming S. A., et al., "Tc-99m-Hexamethylpropyleneamine oxime (Tc-99m-HMPAO) : A new radiopharmaceutical for rCBF imaging," Eur. J. Nucl. Med., 11, A5, 1985.
- Chu S. C., and Berman M., "An exponential method for the solution of systems of ordinary differential equations," Comm. ACM 17, pp. 699, 1974.
- Cowan R. J., and Watson N. E., "Special characteristics and potential single photon emission computed tomography," J. Nucl. Med. 10, pp. 335-344, 1980.
- Crone C., "The permeability of capillaries in various organs as determined by use of the indicator diffusion method," Acta Physiol Scand, 58, pp. 292-305, 1963.
- Dischino D., Welch M., Kilbourn M. R., et al., "Relationship between lipophilicity and brain extraction of C-11- labeled radio pharmaceutical, " J. Nucl. Med. 24, pp. 1030-1038, 1983.
- Eichling J. O., Raichle M. E., Grubb R. L., et al., "Evidence of the limitation of water as a freely diffusible tracer in the brain of the rhesus monkey," Circ. Res. 35, pp. 358-364, 1974.
- Ell J., Costa D. C., Cullum I. D., The clinical application of *rCBF* imaging by *SPECT*, Brier Press Ltd., High Wycombe, 1987.
- Ell J., Hocknell JML, Jarritt P., et al., "A Tc-99m-labeled radiotracer for the investigation of cerebral vascular disease," Nucl. Med. Comm., 6, pp. 437-441, 1985.
- English R. D., and Brown S., *SPECT*, single-photon emission computed tomography : A primer, The society of nuclear medicine publication, NY, NY, 10016, 1986.

- Esser, P., Emission Computed Tomography : Current Trends, Society of Nucl. Med., New York, 1983.
- Garcia J., and Azen S., "A user's experience with a standard non-linear regression program (BMDP3R)," Comput. Programs Biomed. 10, pp. 185-190, 1979.
- Good W. F., Gur D., Yonas H., et al., "Errors in cerebral blood flow determinations by xenon enhanced computed tomography due to estimation of arterial xenon concentrations," Med. Phys. 14, pp. 377-381, 1987.
- Greitz T., Ingvar D., and Widen L., "The metabolism of the human brain studied with positron emission tomography," New York Raven Press, 1983.
- Gur D., Wolfson S. K., Yonas H., et al., "Progress in cerebrovascular disease : local cerebral blood flow by xenon enhancement computed tomography," Stroke 13, pp. 750-758, 1982.
- Harbert J., DaRocha A., The textbook of nuclear medicine vol. 1.: Basic Science, 2nd edition, Lea & Febiger, Philadelphia, PA, 1984
- Hendee W., The physical principles of computed tomography, Little Brown library of radiology, Toronto, 1983.
- Herron J., Molter B., Good B., et al., "Simultaneous mass spectroscopy and thermoconductivity measurements of end-tidal xenon concentration," J. Nucl. Med., 11, pp. 209-212, 1984.
- Herscovitch P., Markham J. Raichle M., "Brain blood flow measured with intravenous $H_2^{15}O$, part I, theory and error analysis" J. Nucl. Med. 24, no. 9, pp. 782-789, 1983.
- Hoffman E. J., Phelps M. E., Mullani N. A., et al., "Design and performance characteristics of a whole body positron transaxial tomography, " J. Nucl. Med., 17, pp. 493-502, 1976.

- Holman B., Lee R. G., Hill T. C., et al., "A comparison of two cerebral perfusion tracers N-isopropyl I-123 p-iodoamphetamine and I-123HIPDM, in the human," J. Nucl. Med. 25, pp. 25-30, 1984.
- Huang S. C., and Phelps M., "A theoretical study of quantitative flow measurements with constant infusion with short lived isotopes," Phy. Med. Biol. 24, pp. 1151-1161, 1979.
- Huang S. C., Carson R. E., and Phelps M. E., "Measurement of local blood flow and distribution volume with short lived isotopes : a general input technique," J. Cereb. Blood Flow, Metab 2, pp. 99-108, 1982.
- Huang S. C., Carson R. E., Hoffman E. J., et al., "Quantitative measurement of local cerebral blood flow in humans by positron computed tomography and O-15 water," J. Cereb. Blood Flow, Metab 3, pp. 141-153, 1983.
- Ingvar D. H., Lassen N. A., "Cerebral function, metabolism and blood flow," Acta Neural Scand 57, pp. 262-269, 1978.
- Jacquez J. A., "Compartmental analysis in biology and medicine," The University of Michigan Press, 1988.
- Kak A. C., Slany M., "Principles of computerized tomographic imaging," IEEE press, pp. 135, 1988.
- Kanno I., Lammertsma A. A., Heather J. D., et al., "Measurement of cerebral blood flow using bolus inhalation of $C^{15}O_2$ and positron emission tomography : description of the method and its comparison with the $C^{15}O_2$ continuous inhalation method," J. Cereb. Blood Flow Metab, 4, pp. 224-234, 1984.
- Kanno I., and Lassen N. A., "Two methods for calculation of regional cerebral blood flow from emission computed tomography of inert gas concentration," J. Comput. Assist. Tomogr., 3, pp. 71-76, 1979.

- Kety S. S., "Measurement of local blood flow by the exchange of an inert diffusible substance," *Methods Med. Res.* 8, pp. 228-236, 1960.
- Kety S. S., "The theory and application of the exchange of inert gas at the lungs and tissues," *Pharmacol. Rev.*, 3, 1, pp. 1-41, 1951.
- Kety S. S., and Schmidt C. F., "The nitrous oxide method for the quantitative determination of cerebral blood flow in man," *J. Clin. Invest.*, 27, pp. 476-482, 1948.
- Kuhl D. E., Barrio J. R., Huang S., et al, "Quantifying local cerebral blood flow by N-isopropyl-p-[123I]iodoamphetamine IMP tomography," *J. Nucl. Med.* 23, pp. 196-203, 1982.
- Kuhl D. E., and Edwards R. Q., "Image separation radio isotope scanning," *Radiology* 80, pp. 653-662, 1963.
- Kuhl D. E., and Edwards R. Q., Ricci A. R., et al., "Quantitative section scanning using orthogonal target correction," *J. Nucl. Med.* 14, pp. 196-200, 1973.
- Kung H. F., and Blau M., "Regional intracellular pH shift: A proposed new mechanism for radiopharmaceutical uptake in brain and other tissues," *J. Nucl. Med.* 21, pp. 147-152, 1980.
- Kung H. F., Molnar M., Billing J., et al., "Synthesis and biodistribution of neutral lipid-soluble Tc-99m complexes that cross the blood-brain-barrier," *J. Nucl. Med.* 25, pp. 326-332, 1984.
- Lammertsma A. A., Jones T., Frackowiak R., et al., "A theoretical study of the steady-state model for measuring regional cerebral blood flow and oxygen utilization using O-15," *J. Comput. Assist. Tomogr.*, 5, pp. 544-550, 1981.
- Lammertsma A. A., Frackowiak R., Hoffman J., et al., "The $C^{15}O_2$ buildup technique to measure regional cerebral blood flow and volume of distribution of water," *J. Cerebral Blood Flow and Meta.* 9, pp. 461-470, 1989.

References

- Lammertsma A. A., Cunningham V., Deiber M., et al., "Combination of Dynamic and Integral Methods for Generating Reproducible Functional *CBF* Images," *J. Cerebral Blood Flow and Meta.* 10, pp. 675-686, 1990.
- Lassen N. A., and Blassberg L., "A fast single photon emission tomography for regional cerebral blood flow studies in man," *J. Compt. Asst. Tomography* 2, pp. 660-661, 1978
- Lassen N. A., Henriksen L., and Paulson O., "Regional cerebral blood flow in stroke by xenon-133 inhalation and emission tomography," *Stroke* 12, pp. 284-288, 1981.
- Lassen N. A., Andersen A., Friberg H., et al., "Validation of ceretec. In: The clinical application of rCBF imaging by SPECT," Brier Press, High Wycombe, pp. 14-18, 1987.
- Lee T. Y., and Yeung I., "A quantitative theory for the measurement of cerebral blood flow with Tc-99m-HMPAO and SPECT," *Phys. Med. Biol.*, 33, Suppl 1, pp. 114, 1988.
- Lee T. Y., Ellis R., Dunscombe P. B., et al., "Quantitative computed tomography of the brain with xenon enhancement: a phantom study with the GE9800 scanner," *Phy. Med. Bio.*, 35, pp. 925-935, 1990.
- Lear J. H., Ackerman R. F., Kameyama M., et al., "Evaluation of I-123 - isopropylidoamphetamine as a tracer for local cerebral blood flow using direct autoradiographic comparison, " *J. Cereb. Blood Flow, Metab.* 2, pp. 175-179, 1982.
- Leonard J. P., Nowotnik D. P., and Neirinckx R. D., " Tc-99m-d, I-HMPAO : A new radio pharmaceutical for imaging regional brain perfusion using SPECT - A comparison with Iodine-123 HIPDM," *J. Nucl. Med.* 27, pp. 1819-1823, 1986.
- Levin V. A., "Relationship of actual/water partition coefficient and molecular weight to the rat brain capillary permeability," *J. Med. Chem.*, 23, pp. 682-684,

- 1980.
- Levy H., Baggott E. A., Numerical Solutions of Differential Equations, Dover, New York, 1950.
 - Lucignani G., Nehlig A., Blasberg R., et al., "Metabolic and kinetic considerations in the use of [125 I]HIPDM for quantitative measurement of regional cerebral blood flow," J. Cereb. Blood Flow, Metab 5, pp. 86-90, 1985.
 - Matsuda H., Oba H., Seki H., et al., "Determination of flow and rate constants in a kinetic model of Tc-99m-HMPAO in the human brain," J. Cereb. Blood Flow, Metab 8, pp. S61-S68, 1988.
 - Mcfarlane Y., Assessment of methods of correction for scatter and attenuation in SPECT imaging, MSc thesis, University of Manitoba, 1988.
 - Mellett B. L., and Veall N., "The measurement for regional cerebral clearance rates in man using xenon-133 inhalation and extracranial recording," Clin. Sci. 29, pp. 179-191, 1965.
 - Meyer E., Heyman M., Yamamoto Y., et al., "Local cerebral blood flow measured by CT after stable Xenon inhalation," Am. J. Neuroradiol., 1, pp. 213, 1980.
 - Meyer E., and Yamamoto Y., "The requirement for constant arterial radioactivity in the $C^{15}O_2$ steady state blood flow model," J. Nucl. Med. 25, pp. 455-460, 1984.
 - Metzler C. M., Elfring G., and McEwen A., A package of computer programs for pharmacokinetic modeling, Biometrics, 30, pp. 562-595, 1974.
 - Mintun M. A., Raichle M. E., Martin W. R., et al., "Brain oxygen utilization measured with O-15 radiotracer and positron emission tomography," J. Nucl. Med. 25, pp. 177-187, 1984
 - Murase. K., Tanada S., Fujita H., et al., "Kinetic behavior of Tc-99m-HMPAO in the human brain and quantification of cerebral blood flow using dynamic

- SPECT," J. Nucl. Med. 33, pp. 135-143, 1992.
- Nakano S., Kinoshita K., Jinnouchi S., et al., "Dynamic SPECT with Tc-99m-HMPAO in meningiomas- A comparison with iodine-123-IMP," J. Nucl. Med. 30, pp. 1101-1105, 1989.
 - Neirinckx R. D., Nowotnik D., Pickett R. D., et al., "Development of a lipophilic Tc-99m complex useful for brain perfusion evaluation with conventional SPECT imaging equipment. In Amphetamines and pH-shift agents for brain imaging: basic research and clinical results," Berlin-New York: Walter de Gruyter, pp. 59-70, 1986.
 - Neirinckx R. D., Canning L. R., Piper I. M., et al., "Tc-99m-d, 1-HMPAO: A new radiopharmaceutical for SPECT imaging of regional cerebral blood perfusion," J. Nucl. Med. 28, pp. 191-202, 1987.
 - Neirinckx R. D., Burke J. F., Harrison R. C., et al., "The retention mechanism of Technetium - 99m - HM -PAO : Intracellular reaction with glutathione," J. of Cerebral Blood Flow and Metab., pp. S4-S12, 1988.
 - Nickel O., Nagele-Wohrle B., Ulrich P., et al., "rCBF quantification with Tc-99m-HMPAO - SPECT : Theory and first results," Eur. J. Nucl. Med. 15, pp. 1-8, 1989.
 - Nowotnik D. P., Canning L. R., Cumming S. A., et al., "Development of a Tc-99m-labeled radio pharmaceutical for cerebral blood flow imaging," Nucl. Med. Comm. 6, pp. 499-506, 1985.
 - Nudelman S., Pathon D., Imaging for medicine, Plenum Press, New York, NY, 1, 1980.
 - Obreist W. D., Thompson H. K., King C., et al., "Deterioration of regional cerebral blood flow by inhalation of xenon-133.," Circulate RES. 20, pp. 124-135, 1967.

- Obreist W. D., Thompson H. K., Wong H. S., et al., "Regional cerebral blood flow estimated by xenon-133 inhalation," *Stroke* 6, pp. 245-256, 1975.
- Papoulis A., *Probability, random variables, and stochastic processes*, Mac Graw Hill Book Company, 1965.
- Phelps M. E., Mazziotta C., Huang S., et al., "Study of cerebral function with positron computed tomography," *J. cereb. Blood. Flow, Metab* 2, pp. 113-163, 1982.
- Posner J. B., "New techniques of cerebral blood flow measurements," *Stroke* 3, pp. 227-237, 1972.
- Raichle M. E., Marting W., Herscovitch P. et al., "Brain blood flow measured with intravenous $H_2^{15}O$, part II, implementation and validation," *J. Nucl. Med.* 24, pp. 790-798, 1983.
- Rapin J. R., Lepponcin-Lafitte M., Duterte D., et al., "Iodoamphetamine as a new tracer for local cerebral blood flow in the rat : comparison with isopropylidoamphetamine," *J. Cereb. Blood Flow, Metab* 4, pp. 270-274, 1984.
- Ravert H. T., Burns H. D., Heindel N. D., et al., "Synthesis of neutral, lipid soluble technetium complex of bis (2-mercaptoethyl) amines," *J. Nucl. Med.* 24, pp. p10, 1983.
- Robertson J. S., "Theory and use of tracers in determining transfer rates in biological systems, " *American Physical Society*, 37, pp. 133-153, 1957.
- Sakurada O., Kennedy C., Jehle J., et al., "Measurement of local cerebral blood flow with iodo[14-C]antipyrine," *Am. J. Physical* 234, pp. H59-H66, 1978.
- Sharp P. F., Smith F. W., Gemmell H. G., et al., "Tc-99m-HMPAO stereoisomers as potential agents for imaging regional cerebral blood flow : Human volunteer studies," *J. Nucl. Med.* 27, pp. 171-177, 1986.

- Sorenson J. A. Phelps M. E., Physics in nuclear medicine, Grune and Stratton Inc. New York, 1980.
- Subramanyam R., Alpert N. M., Hoop B., et al., "A model for regional cerebral oxygen distribution during continuous inhalation of $C^{15}O$ and $C^{15}O_2$," J. Nucl. Med. 19, pp. 48-53, 1978.
- Ter-Pogossian M. M., "Special characteristics and potential for dynamic function studies with PET," Sem Nucl. Med. 11, pp. 13-23, 1981.
- Tramposch K. M., Kung M., and Blau M., "Radioiodine labeled N, N-dimethyl - N- (2- hydroxyl - 3 - allyl - 5 - iodobenzyl) - 1,3 - propanediamines for brain perfusion imaging," J. Med. Chem., 28, pp. 121-125, 1983.
- Troutner D. E., Volkert W. A., Hoffman T. J., et al., "A tetradentate amine complex of Tc-99m," J. Nucl. Med. 24, pp. 10-14, 1983.
- Troutner D. E., Volkert W. A., Hoffman T. J., et al., "A neutral lipophilic complex of Tc-99m with multidentate amine oxime," Int. J. Appl. Radio., 35, pp. 467-470, 1984.
- Vallabhajosula S., Zimmerman R., Picard M., et al., "Tc-99m-ECD : A new brain imaging agent *in-vivo* kinetics and biodistribution studies in normal human subjects," J. Nucl. Med. 30, pp. 599-604, 1989.
- Volkert W. A., Hoffman T. J., Seger R. M., et al., "Tc-99m-PnAo; a potential brain radio pharmaceutical," Eur. J. Nucl. Med. 9, pp. 511-516, 1984.
- Walovitch R. C., Williams S. J., Morgan R. A., et al., "Pharmacological characterization of TC-99m-ECD in non-human primates as a new agent for brain perfusion imaging [Abstract]," J. Nucl. Med. 29, pp. 788, 1988.
- Wartak J., Clinical pharmacokinetics : A modern approach to individualized drug theory, New York, NY., 1983.

References

- West J. B., Dollery C. T., "Uptake of O-15-labelled CO_2 compared with C-11-labelled CO_2 in the lung," J. Appl. Physiol., 17, pp. 9-13, 1962.
- Winchell H. S., Baldwin R. M., and Lin T. H., "Development of I-123-labeled amines for brain studies localization of I-123 iodophenylalkyl amines in the rat brain," J. Nucl. Med. 21, pp. 940-942, 1980.
- Winchell H. S., Horst W. D., Braun L., et al., "N-Isopropyl(I-125)p-iodoamphetamine: Single pass brain uptake and washout: binding for brain synaptosomes; and localization in dog and monkey brain," J. Nucl. Med. 21, pp. 947-952, 1980.
- Worsley B. H., and Lax L., Proc. 2nd Conf. Computing Data-Processing Soc. Can., University of Toronto Press, pp. 158-164, 1960.